Microbially-catalyzed conjugation of GABA and tyramine to bile acids

Michael W. Mullowney[1], Aretha Fiebig[2], Matthew K. Schnizlein [2], Mary McMillin[1], Jason Koval[3], David Rubin[3], Sushila Dalal[3], Mitchell L. Sogin[4], Eugene B. Chang[3], Ashley M. Sidebottom[1*], Sean Crosson[2*]

[1]Duchossois Family Institute, University of Chicago, 900 E. 57th St, Chicago, IL, 60637, USA
[2]Department of Microbiology and Molecular Genetics, Michigan State University, East Lansing, Michigan, USA
[3]Department of Medicine, University of Chicago, 900 E. 57th St, Chicago, IL, 60637, USA
[4]Marine Biological Laboratory, Woods Hole, MA USA
*address correspondence

Abstract
Bile acids (BAs) are cholesterol-derived molecules in the human gut that aid in digestion and nutrient absorption, regulate host metabolic processes, and influence gut microbiome composition. Both the host and its microbiome contribute to enzymatic modifications that shape the chemical diversity of BAs in the gut. Several bacterial species have been reported to conjugate standard amino acids to BAs, but it was not known if bacteria conjugate other classes of amines to BAs. We show that *Bacteroides fragilis* strain P207, isolated from a bacterial bloom in the J-pouch of a patient with ulcerative colitis (UC) pouchitis, conjugates standard amino acids and the neuroactive amines γ-aminobutyric acid (GABA) and tyramine to deoxycholic acid. We extended our analysis to other human gut isolates and identified bacterial species that conjugate GABA and tyramine to primary and secondary BAs, and further identified diverse BA-GABA and -tyramine amides in human stool. A time-series metabolomic analysis of UC J-pouch contents revealed a lack of secondary bile acids and a shifting BA conjugate profile before, during and after onset of pouchitis, including temporal changes in several BA-GABA amides. Treatment of pouchitis with ciprofloxacin was associated with a marked reduction of nearly all BA amides in the J-pouch. Our study expands the known repertoire of conjugated bile acids produced by bacteria to include BA conjugates to the neuroactive amines GABA and tyramine, and demonstrates that these molecules are present in the human gut.

Importance
Bile acids (BAs) are modified in multiple ways by host enzymes and the microbiota to produce a chemically diverse set of molecules that assist in the digestive process and impact many physiological functions. This study reports the discovery of bacterial species that conjugate the neuroactive molecules, GABA and tyramine, to primary and secondary BAs. We further present evidence that BA-GABA and BA-tyramine conjugates are present in the human gut, and document a shifting BA-GABA profile in a human pouchitis patient before, during and after inflammation and antibiotic treatment. GABA and tyramine are potent neuroactive molecules and common metabolic products of the gut microbiota. GABA- and tyramine-conjugated BAs may influence receptor-mediated regulatory mechanisms within the gastrointestinal tract and absorption of these molecules and their entry into the enterohepatic circulation may impact host physiology at distal tissue sites. This discovery defines new conjugated bile acids in the human gut.

Introduction

Bile acids are produced from cholesterol in the liver through a multi-step enzymatic process [1]. The primary bile acids (PBAs) in humans, cholic acid (CA) and chenodeoxycholic acid (CDCA), are synthesized in hepatocytes where they are enzymatically conjugated to the amine group of glycine or taurine to form an amide bond [2, 3]. After secretion into bile and release into the intestinal lumen, members of the gut microbiota deconjugate glycine or taurine from PBAs and can chemically modify the sterol core to yield secondary bile acids (SBAs) of various chemical forms [4, 5]. Bile acids are eventually resorbed in the intestine and returned to the liver through enterohepatic circulation where they can be re-conjugated or repaired in the hepatocyte [6].

Recent studies have shown that at least 15 of the 20 standard protein-encoding amino acids can be conjugated to CDCA, CA or deoxycholic acid (DCA) by a range of bacteria that reside in the gut including species of the genera *Bacteroides*, *Lactobacillus*, *Bifidobacterium*, *Enterocloster*, *Ruminococcus*, and *Clostridium* [7-9]. This discovery has expanded the known chemical repertoire of bile acids that may enter circulation. The impact of microbially-conjugated bile acids on microbiome composition and host physiology are not known, but the ability of bile acids to affect mammalian physiology through a range of receptors is well established. In select cases, regulation of signal transduction is affected by specific conjugated forms of bile acids [10]. For example, regulation of Takeda G protein-coupled receptor 5 (TGR5) and farnesoid X receptor (FXR), which can function as bile acid receptors, is

influenced in part by the chemical identity of the amino acid that is conjugated to the sterol core [9, 11].

In ulcerative colitis (UC) patients who have undergone ileal pouch anal anastomosis (IPAA), a dysbiosis-induced deficiency of SBAs including DCA and lithocholic acid (LCA) is proposed to cue to an inflammatory state that can lead to pouchitis [12]. While it remains uncertain if microbial-mediated bile acid conjugation reactions directly modulate DCA and LCA levels in these patients, we have previously found dominant *Bacteroides fragilis* strains that constitute over 50% of the bacterial population in the ileoanal pouch (or J-pouch) of UC pouchitis patients before the emergence of inflammation [13]. Given this, our study aimed to investigate the capability of one of these dominant *B. fragilis* strains to chemically transform primary and secondary bile acids. Furthermore, we aimed to delineate the bile acid profile over time in the human patient from whom this particular *B. fragilis* strain was isolated, post-surgical functionalization of the J-pouch.

Here, we report that a *B. fragilis* strain (P207) isolated from a patient suffering from UC pouchitis [13] conjugates glycine (Gly), alanine (Ala), phenylalanine (Phe), γ-aminobutyric acid (GABA), and tyramine to DCA *in vitro*; conjugation to CA was limited to glycine. *B. fragilis* P207 deconjugates glycodeoxycholate (GDCA) to produce DCA, and can subsequently produce Ala-, Phe-, GABA-, and tyramine-DCA conjugates from the deconjugated bile acid. Thus, *B. fragilis* P207 produces a chemically diverse pool of conjugated bile acids *in vitro*, including the novel GABA-DCA and tyramine-DCA products, starting from either DCA or GDCA. A time-series metabolomic analysis of stool from this pouchitis patient before and after onset of pouch inflammation revealed a lack of secondary bile acids across all time points and the presence of multiple bile acid-amine conjugates, the levels of which were strongly reduced following antibiotic treatment. Among the BA-conjugated amines detected in these stool samples, or in samples collected from healthy donors, were GABA and tyramine. Our results expand the known set of microbially-catalyzed bile conjugation reactions, and have identified novel bile acid conjugates to GABA and tyramine in the human gut. Both GABA [14] and tyramine [15] are common products of microbial metabolism and are potent neuromodulatory molecules. Flux of these amines in the gut due to microbe-catalyzed conjugation to bile acids may impact host physiology.

Results

Chemical transformation of primary and secondary bile acids by *B. fragilis* P207

B. fragilis P207 was incubated in supplemented Brain Heart Infusion (BHIS) broth with and without deoxycholic acid (DCA) (0.01% w/v), and samples were analyzed by ultra-high-performance liquid chromatography tandem high resolution mass spectrometry (UHPLC-MS^2). Fragmentation-based networking of the mass spectrometry data identified derivatives of DCA from a set of candidate conjugates presented in Table S1. This metabolomic approach provided evidence for five amide-linked conjugates of DCA, which were only present in the spent media of cultures that contained both *B. fragilis* P207 and DCA. Fragmentation patterns consistent with DCA-alanine, DCA-glycine, DCA-phenylalanine, DCA-tyramine, and DCA-γ-aminobutyric acid (DCA-GABA) were identified (Figure 1). To our knowledge, this is the first report of GABA or tyramine conjugation to a bile acid. We sought to validate the production of these bile acid-amine conjugates by *B. fragilis* P207 by supplementing the broth with isotopically labeled versions of each of these amines. Specifically, we supplemented broth containing strain P207 and deoxycholic acid (0.01% w/v) with 1 mM of either isotopically labeled 4-aminobutyric acid ($^{13}C_4$, 97-99%), L-alanine ($^{13}C_3$, 99%), glycine ($^{13}C_2$, 99%; ^{15}N, 98%+), L-phenylalanine (D_8, 98%), or tyramine:HCl (1,1,2,2-D_4, 98%). Analyses of spent media from each of these conditions revealed the expected intact mass (MS^1) and fragments (MS^2) for all five DCA conjugates (<0.48 ppm error for all MS^1 ions and <6 ppm error for all MS^2 ions representing predicted structures), as well as the expected mass shifts when media was supplemented with the isotopically labelled precursors (Figure 2; Figures S1–S5). Mass spectrometry evidence for production of these conjugates is presented in Supplemental Results.

To assess chemical specificity of bile acid conjugation by *B. fragilis* P207, we further tested for production of cholic acid (CA) conjugates. Mass spectrometry analyses revealed trace levels of DCA in the BHIS growth media and traces of DCA and GCA in the starting CA reagent, but GCA levels were clearly enhanced by incubation of CA (0.01% w/v) with *B. fragilis* P207 (Figure 3A). Simultaneous incubation of CA and DCA (0.01% w/v total) with strain P207 showed similar production of the same five DCA conjugates described above. Thus, the addition of CA did not apparently impact P207-dependent production of the five DCA conjugates over this timescale (Figure 3B). We conclude that strain P207 prefers DCA as a conjugation substrate over CA in BHIS medium.

Lucas and colleagues have demonstrated that modification of CA into the secondary bile acid, 7-oxo-DCA, is robust and widespread across several species of *Bacteroides*, while production of DCA from CA was limited to *Bacteroides vulgatus* [8]. We did not observe increased DCA levels when P207 was incubated with CA, nor did we observe production of any DCA conjugates from CA indicating that *B. fragilis* P207 does not catalyze production of DCA from CA under these conditions. The relative abundances of bile acid conjugates across replicate experiments are presented in Figure S6, and a complete presentation of mass spectrometry evidence for each of the conjugates is available in the supplemental material.

P207 catalyzed deconjugation and reconjugation of amines to DCA

Given that some bacteria can deconjugate glycine and taurine from secreted bile acids, we tested whether *B. fragilis* P207 is able to produce the DCA conjugates described above using glycodeoxycholate (i.e. GDCA) as an initial substrate. *B. fragilis* P207 was incubated in BHIS broth with and without GDCA (0.01% w/v), and culture samples were analyzed by UHPLC-MS^2. We observed trace contaminants DCA and glycocholic acid (GCA) in

the growth medium and bile acid reagent, but incubation of GDCA with strain P207 resulted in decreased GDCA and increased DCA levels providing evidence that *B. fragilis* P207 has GDCA deconjugation activity (Figure 4). We further observed production of the DCA conjugates described above (GABA, tyramine, alanine, phenylalanine) from GDCA when strain P207 was present (Figure 4). We conclude that *B. fragilis* P207 can produce all the DCA conjugates described in the section above when either DCA or GDCA is present as an initial substrate.

GABA production by *B. fragilis* P207 is induced by deoxycholate

The observation of bile acid conjugation to a distinct set of amines *in vitro* raised a question about the levels of these amines in the culture medium. To measure specific amine-containing compounds in *B. fragilis* P207 cultures before and after exposure to DCA we employed gas chromatography-mass spectrometry (GC/MS) on the same culture samples from which DCA conjugates were initially identified. Among the five amines conjugated to DCA, alanine and phenylalanine were most abundant, followed by glycine at levels 15- to 40-fold lower. Tyramine and GABA were present at levels approximately 10-fold less than glycine (Figure 5). Relative amine abundances did not, therefore, correlate with the levels of their respective DCA conjugates produced *in vitro* (Figure S6).

Notably, when DCA was added to the culture medium, a significant increase in GABA was observed; glycodeoxycholic acid (GDCA) addition did not have this effect on microbial GABA production. The relative concentrations of other conjugated amines (i.e. alanine, phenylalanine, glycine, and tyramine) was unchanged across all treatment conditions (Figure 5). *Bacteroides* species in the human gut are known to produce GABA from either glutamate or glutamine, particularly under pH stress conditions [16]. Given the increase in GABA following DCA treatment, we expanded our GC/MS analysis to include glutamine, glutamate, as well as other naturally occurring amino acids. DCA treatment did not impact glutamine levels but it did lead to a modest reduction in glutamate concentrations, which is consistent with a model whereby DCA stimulates *B. fragilis* P207 to convert glutamate into GABA (Figure S7). However, DCA was recently reported to induce increased expression of glutamate dehydrogenase (gene locus *PTOS_003163*) in *B. fragilis* P207 [17], suggesting that the metabolite flux involving glutamate is modulated in multiple ways by DCA. Overall, cultivation of *B. fragilis* P207 did not greatly affect the levels of amino acids in BHIS medium, with the exception of asparagine and aspartate. Concentration of these two amino acids decreased approximately 50- and 10-fold, respectively, suggesting they serve as primary nutritional substrates for *B. fragilis* P207 in BHIS medium.

Defining the bile acid conjugate profiles of a pouchitis patient and healthy donors

To test if the bile acid conjugates produced by *B. fragilis* P207 *in vitro* are present in the human gut, we prepared extracts of stool samples from pouchitis patient 207 collected at timepoints before and after onset of pouchitis, and during antimicrobial treatment [13]. Metabolomic data from this patient were compared to UHPLC-MS^2 data from 21 healthy donor stool samples. Patient 207 and healthy donor stool contained a complex mixture of bile acids (Table S2). Unlike healthy donors, which contained expected high levels of DCA, patient 207 lacked DCA across all time points (Figure S8 and Table S2). This result is congruent with a reported deficiency in secondary bile acids in UC pouches [18]; we infer that this pouchitis patient was missing the microbial 7α-dehydroxylating activity required to produce DCA. The primary bile acids chenodeoxycholate (CDCA) and CA were abundant across all time points in patient 207, at levels that were ≈60 times higher on average than observed in the 21 healthy donor samples ($p < 0.0001$). Amine conjugates to CA and CDCA, including putative GABA conjugates, were present in patient 207 (Figure 6 and Figure S8-S10) at levels that were higher than healthy patients on average (Table S2). We detected several amines conjugated to a bile acid core that had an *m/z* corresponding to DCA or its isomers (Figure 6 and Figure S8). Considering the lack of DCA and abundance of CDCA in patient 207, we presume many of these species are CDCA conjugates though the exact chemical identity of these products remains undefined. Bile acid conjugates to tyramine were not observed in patient 207, though we did find evidence for bile acid-tyramine conjugates in 7 healthy donor samples indicating that tyramine can exist in a bile conjugated form in the human gut (Table S2 and Figure S11).

B. fragilis strain P207 dominated the pouch ecosystem of patient 207 from 182 to 434 days after surgical functionalization of the ileal pouch (i.e. IPAA) [13]. Normalized levels of bile acids, including the primary bile acids CA and CDCA, were low at 124 days and 236 days after IPAA. There was a marked increase in unconjugated CA and CDCA and bile acid conjugates at 355 days post-functionalization, and levels trended upward by 482 days when the patient was diagnosed with pouchitis and initiated a course of antibiotic therapy (ciprofloxacin) (Figure S9 and S12). The contribution of *B. fragilis* strain P207 to the production of particular bile acid conjugates at these time points is not known, but the *in vitro* conjugation data presented above indicate that observed CA conjugates (other than glycocholate) are not produced by *B. fragilis* P207 (Figure 2). At a follow-up visit 525 days post-IPAA, ciprofloxacin treatment had resulted in a large reduction of the pouch microbiome census and pouch inflammation was resolved [13]. Bile acid analysis shows that levels of conjugated and unconjugated bile acids were sharply reduced at this time point during antibiotic treatment except for select low abundance conjugates of CA and DCA isomers to glycine and GABA, which increased (Table S2, Figures S9 and S12). After the conclusion of ciprofloxacin treatment (at 601 days), the patient again exhibited pouch inflammation. By this visit, the dominant species of the pouch had completely shifted from *B. fragilis* P207 to *Bacteroides ovatus* [13]. This change in the pouch microbiome after antibiotic treatment was correlated with a change in the bile acid conjugate profile, with distinct CA and DCA isomer conjugates to GABA and glycine increasing (Table S2, Figures S9 and S12)

Our data provide evidence that both GABA and tyramine are present in bile-conjugated forms in the human gut (Figure 6, Figures S10-S11; Table S2). The direct impact of *B. fragilis* P207 on the bile acid profile of pouchitis patient 207 is not resolved by our data, though the lack of CA conjugation activity of this strain *in vitro* indicates that the CA conjugates present in this patient are produced though other host- or microbiome-dependent mechanisms. Our data further show an absence of DCA in this pouchitis patient, document a shifting bile acid profile leading up to the development of pouchitis, and provide evidence that patient bile acids are strongly impacted by ciprofloxacin treatment during pouch inflammation.

Conjugation of GABA and tyramine to CA by human gut isolates

Metabolomic analysis of stool samples from pouchitis patient 207 and healthy human donors revealed a complex mixture of known and previously unreported bile acid conjugates, including CA conjugates to GABA and tyramine (Figure 6). As discussed above, conjugates to CA are likely produced by microbes other than *B. fragilis* P207 (Figure 3). To discover bacteria that can produce these novel CA conjugates, we inspected the genomes of a collection of human gut isolates for genes that encode predicted N-terminal nucleophilic cysteine hydrolase (Ntn) enzymes, which includes known choloylglycine hydrolases (Conserved Domain Database accession cd01902; [19]). Recent studies report that this class of enzymes can function to both deconjugate and conjugate bile acids [20, 21]. Indeed, *B. fragilis* P207 encodes an Ntn hydrolase (WP_005817456.1) and we predicted that other strains encoding these enzymes may conjugate GABA or tyramine to CA *in vitro*. We selected a phylogenetically diverse group of human patient isolates that were also predicted to encode an Ntn hydrolase, including *Mediterraneibacter gnavus* MSK15.77 (WP_004614568.1), *Bifidobacterium longum* DFI.2.45 (WP_007052221.1), and *Bacteroides ovatus* MSK22.29 (which encodes three Ntn paralogs: WP_217723859.1, WP_004308262.1, and WP_004323538.1) (Figure S13). As a control, we identified a strain that does not encode a predicted Ntn bile salt hydrolase, *Lachnoclostridium scindens* SL.1.22. All three Ntn-encoding gut isolates produced putative GABA conjugates to CA, and *M. gnavus* and *B. longum* cultures contained a product that had an MS^2 fragmentation pattern consistent with CA-tyramine (Figure 7 and Figure S14). *L. scindens* cultures did not contain CA conjugates.

We further investigated if these strains could conjugate amines to DCA and detected conjugates of alanine, phenylalanine, and GABA to DCA in the culture extracts of *M. gnavus*, *B. longum*, and *B. ovatus*. Additionally, DCA-tyramine conjugates were identified in *M. gnavus* and *B. ovatus* cultures (Figure 7). Although the *L. scindens* SL.1.22 genome does not encode a predicted Ntn family/bile salt hydrolase (BSH) enzyme, we observed low levels of DCA-Phe and DCA-Ala conjugates in its culture extract when this strain was incubated with 0.01% (w/v) DCA. The specific gene(s) responsible for DCA conjugation in our *L. scindens* cultures remain unidentified.

Discussion

On the mechanism of microbial bile acid conjugation

B. fragilis P207 produces a suite of DCA amidates *in vitro*, in which the bile acid carboxylate group is conjugated to the amine group of select amino acids and bioactive amines. Biosynthesis of bile acid amidates by gut microbes is a recent discovery [8, 9], and there is now genetic and biochemical evidence that bacterial bile salt hydrolase (BSH) enzymes can catalyze aminoacyl transfer to bile salts [20, 21]. Thus, BSH proteins have significant N-acyl transferase activity in addition to their long-established function as hydrolases [22]. While microbial conjugation of bile acids to the α amino group of amino acids has been described, our data provide evidence that an activity encoded by P207 enables conjugation of the primary amine groups of GABA and tyramine to DCA. DCA conjugate biosynthesis was evident when culture broth was supplemented with either unconjugated (DCA) or conjugated (GDCA) bile acids, which supports a model in which P207 first deconjugates GDCA and then generates DCA amidates from the deconjugated product.

The *B. fragilis* P207 genome (GenBank accession CP114371) encodes a single predicted BSH (gene locus *PTOS_003312*) that shares 80% identity with BT2086, a protein that has demonstrated BSH activity in *B. thetaiotaomicron* [23]. PTOS_003312 is 99% identical to the BSH of *B. fragilis* strain 638R (locus *BF638R_3310*), which promotes deconjugation of primary bile acids in the gut of germ-free mice [24]. In light of recent *in vitro* biochemical data showing that purified *Clostridium perfrigens* [20] and *Bifidobacterium longum* [21] BSH enzymes produce bile acid amides from both unconjugated (CA) and conjugated (taurocholic acid; TCA) bile acids, it seems most likely that PTOS_003312 of *B. fragilis* P207 catalyzes the production of the five bile acid conjugates reported here, using either GDCA or DCA as substrates, though we cannot rule out the possibility that these products arise from the activity of multiple enzymes. P207 demonstrates a clear preference for bile acid amide production from the secondary bile acid, DCA, over primary bile acid CA, which differ only by a single hydroxyl group at C-7. Based on this result, we infer that the C-7 position of the sterol core is important for bile acid substrate interaction with the transforming enzyme(s) of strain P207 (likely PTOS_003312).

The detection of DCA conjugation to the primary amine groups of GABA and tyramine was unexpected and raises questions about the mechanism of bile acid conjugation given the relative difference in nucleophilicity and steric accessibility of the primary amine groups of tyramine and GABA (pKa $\approx$ 10.5-11.0 in aqueous solvent) and the typical α amino group (pKa $\approx$ 9-9.5) of amino acids. Considering the diversity in primary structure of BSH enzymes and the selectivity of BSH enzymes for particular steroidal cores across *Bacteroides* spp. [23], it is likely that structural differences in the active site or other regions of the conjugating enzyme [25] will determine whether primary amine groups, such as those on GABA and tyramine, form amide bonds with bile acid(s). It is plausible that other bioactive amines present in the gut can be conjugated to bile acids and *B. fragilis* P207, *M. gnavus* MSK15.77, *B.*

longum DFI.2.45, and *B. ovatus* MSK22.29 provide models to begin investigation of this hypothesis.

The benefit of bile acid conjugation to *B. fragilis* and other microbes, if any, is not clear. *B. fragilis* P207 can deconjugate GDCA and produce a variety of conjugated compounds from the deconjugated bile acid substrate (DCA). Unconjugated primary and secondary bile acids are often more toxic *in vitro* than the amino acid-conjugated forms [26-28]. We assessed the relative toxicity of unconjugated and conjugated CA and DCA to *B. fragilis* P207 and demonstrated that growth of this strain is more sensitive to CA and DCA than glycocholate and glycodeoxycholate (Figure S15). We further observed that the secondary bile acid, DCA, is more toxic than CA. The ability to conjugate amino acids effectively detoxifies DCA *in vitro* and may therefore influence the impact of bile salts on *B. fragilis* physiology *in vivo*.

Broader connections of bile acid conjugation to mammalian physiology

This study defines the temporal bile acid profile of the J-pouch of a pouchitis patient, before during, and after inflammation including a period of antibiotic therapy, and draws comparisons of this profile to healthy individuals. Healthy human donors presented expected high levels of DCA, while the pouchitis patient was severely DCA deficient. This aligns with previous observations of reduced secondary bile acids in UC pouches [18]. As expected for a patient with diminished secondary bile acid production, the primary bile acids, CDCA and CA, were significantly elevated in the pouchitis patient. Furthermore, unique amine conjugates to CA and CDCA, particularly novel GABA conjugates, were identified in in this patient. Our *in vitro* analyses of *B. fragilis* P207, which was isolated from this patient, and of other human gut microbiome isolates has demonstrated that bile acid conjugates to GABA and tyramine observed in stool can be produced by multiple bacterial genera. Changes in the levels of bile acids leading up to pouchitis onset, coupled with the marked influence of ciprofloxacin treatment on the bile acid profile (Figures S9 and S12), underscore the complex interplay between gut microbiota, host factors, and therapeutic interventions on the bile acid profile of humans.

The bioactive amines, GABA and tyramine, are potent regulators of mammalian physiology. Both molecules are produced by microbes that inhabit the gut microbiome, including Bacteroidetes [16]. GABA has a well-recognized role in the regulation of gut physiology [29]. GABA-producing *Bacteroides* have been shown to increase steady-state levels of GABA in the intestines of mono-associated germ-free mice [30]. Conjugation and subsequent uptake of bile acid-GABA amidates into enterohepatic circulation may impact GABAergic signaling in the gut and possibly at other distal tissue sites. Our data indicate that bile acid exposure can enhance microbial GABA production (Figure 5). Through UHPLC-MS^2 analysis, we identified GABA-bile acid conjugates in human stool samples, and showed that these levels change with antibiotic treatment in a human pouchitis patient (Table S2, Figure S9 and S12).

Tyramine is a product of tyrosine catabolism but is also present at high levels in a variety of foods. Steady-state tyramine levels in human tissue are typically low due to the activity of monoamine oxidase A, but can be modulated in patients treated with monoamine oxidase inhibitors [31]. Trace amine associated receptors (TAARs), with which tyramine can interact, have been reported in human enterochromaffin (EC) cells of the human gut [32], though the impact of dietary and microbiome-derived tyramine of TAAR signaling in the gut is not known. Tyramine-bile acid amidates in human patients likely vary as a function of diet and other factors and vary geographically along the digestive tract depending on the amount of microbial tyramine production and the spectrum of bile acid conjugating activity conferred by the host microbiome at particular foci.

The impact of specific bile acid amidates reported here on signaling through bile acid receptors is an interesting future area of investigation. Bile salt hydrolase (BSH) activity of non-enterotoxigenic *Bacteroides* spp. was recently reported to potentiate obesity-related colorectal cancer progression in a mouse model [33]; this effect was attributed in part to enhanced TGR5 signaling as a result of increased levels of deconjugated DCA and lithocholic acid in the colon. Certainly, gut microbe BSH activity can lower the level of deconjugated bile acids in the gut. However, it is important to consider that BSH activity results in a spectrum of unconjugated and conjugated bile acids [20, 21], including compounds reported here. The effect of these compounds on signaling from bile acid receptors may shape host physiology, disease, and health.

Materials and Methods

Cultivation of bacteria in the presence of bile acids

B. fragilis P207 (NCBI locus NZ_CP114371) was cultivated in Brain-Heart infusion medium supplemented with hemin (BHIS) containing either 0.01% (w/v) deoxycholic acid (DCA), cholic acid (CA) or glycodeoxycholic acid (GDCA) that was inoculated from a saturated starter culture (≈1.0 OD_{600}), back-diluted 1:10. Cultures were grown for 24 hours; 1 ml of culture was removed and flash frozen for subsequent metabolomic analysis. *Mediterraneibacter gnavus* MSK15.77 (NCBI accession NZ_JAAIRR010000000), *Bacteroides ovatus* MSK22.29 (NCBI accession NZ_JAHOCX010000000), *Bifidobacterium longum* DFI.2.45 (NCBI accession NZ_JAJCNS010000000), and *Lachnoclostridium scindens* SL.1.22 (NCBI accession GCA_020555615.1) were also cultivated in BHIS. Briefly, starter cultures were inoculated from frozen glycerol stocks and grown anaerobically at 37˚C overnight to ≈1.0 OD_{600}. These cultures were diluted to ≈0.005 OD_{600} in 1 ml of plain BHIS or BHIS containing 0.01% (w/v) DCA or CA in a 96-well deep well plate. The plate was incubated at 37˚C anaerobically for 20 hours and then frozen at -80˚C for subsequent metabolomic analysis.

Untargeted metabolomic approach to detect bile acid conjugates in vitro

Bacteria culture supernatants were lyophilized followed by 2X concentration in 100% methanol (containing

internal standards). Samples were then centrifuged at −10 °C, 20,000 x *g* for 15 min to generate supernatants for subsequent metabolomic analysis. All ultra-high-performance-liquid chromatography-mass spectrometry (UHPLC-MS) analyses were performed using a Thermo Scientific Vanquish Flex UHPLC coupled with an IQ-X mass spectrometer (Thermo Fisher Scientific). Reversed-phase chromatography was performed at a 300 µL • min-1 flow rate on a Waters CORTECS T3 C18 RP-UHPLC column (100 × 2.1 mm inner diameter, 1.6 µm particle size, 120 Å pore size (1 Å = 0.1 nm)). Mobile phase A was 5% acetonitrile in water with 0.1% formic acid and mobile phase B was acetonitrile with 0.1% formic acid. The chromatographic method used was an isocratic 20% mobile phase B (99.9% acetonitrile, 0.1% formic acid) for 0.2 min, followed by a gradient of 20 to 97% mobile phase B for 11.8 min with a wash of 97% mobile phase B for 1.15 min. All samples were analyzed using positive ionization. Flow from the UHPLC was ionized with the heated electrospray ionization (HESI) source set to 3400 V, ion transfer tube temp set to 200 °C, vaporizer temperature set to 400 °C, and sheath, aux and sweep gases set to arbitrary values of 40, 5, and 1, respectively. Data for MS^1 were acquired using a maximum inject time of 50 ms, a normalized AGC target of 25%, a 300–1700 m/z quadrupole scan range, and a resolution of 60,000. All tandem MS^2 mass spectral data were acquired using a 1.5 m/z quadrupole isolation window, a maximum inject time of 22 ms, a normalized AGC target of 20%, and a resolution of 15,000. Each of the metabolite ions of interest were added to an inclusion list for MS^2 fragmentation by a normalized higher-energy collisional dissociation energy of 30%. Data analysis was performed using FreeStyle software (version 1.8 SP2, Thermo Scientific), MZmine 2.53 [34] GNPS platform tools Feature-Based Molecular Networking (FBMN) release 28.2 and Mass Search Tool (MASST) release 29, [35-37], and GraphPad Prism version 9.4.1 for Windows (GraphPad Software, San Diego, California, USA, www.graphpad.com). Areas under the curve (AUC) were normalized to the average of D_4-taurocholate and D_4-taurodeoxycholate areas under the curve and multiplied by 1000:

$$\text{normalizedAUC} = (\text{peak}_{AUC} / ((D_4\text{-}TC_{AUC} + D_4\text{-}TDC_{AUC})/2)) \times 1000$$

Data processing and molecular networking

Data-dependent mass spectrometry data files were processed using MZmine 2.53 and the Feature-Based Molecular Networking function in the Global Natural Products Social Molecular Networking (GNPS) environment to identify and network spectral features while also matching generated data to publicly available library spectra. MZmine was used to detect MS^1 and MS^2 peaks, build deconvoluted extracted ion chromatograms, group isotopes, and match the resulting features across samples, accounting for retention time drift across injections. Features within each sample were then normalized by dividing peak area by the average peak area of the internal standards in that sample. Features that are found in solvent and method blank controls were then eliminated. The aligned feature lists were then exported for analysis using the FBMN tool within the GNPS platform.

FBMN was performed with precursor ion mass tolerance and fragment ion mass tolerance both set to 0.02 Da, minimum matched fragment ions set to six, networking cosine score set to > 0.7, library cosine score set to > 0.7, and minimum library shared peaks set to six. A visualization of the network was constructed in Cytoscape by drawing edges between scan nodes with a cosine similarity > 0.7. The network was manually analyzed to identify ions that occurred only in samples containing BHIS, a bacterial strain, and DCA or CA, with a particular focus on those that occurred within the same molecular families as our bile acid internal standards and other nodes that matched to library entries of known bile acids. Nodes in the molecular network were also checked against a list of predicted *m/z* values for hypothesized amine-containing conjugates presented in Table S1. Data files were also manually analyzed for MS^2 scans containing characteristic DCA core fragments at *m/z* 215.1794 and *m/z* 339.2682 (observable in Figures S1-S5) to identify metabolite ions that may not have been clustered in the molecular network due to falling below networking thresholds.

Isotopically labeled amine feeding experiments

To test for conjugation of isotopically labeled amines to DCA by *B. fragilis* P207, 1 ml cultures containing 1 mM (final concentration) of either 4-aminobutyric acid ($^{13}C4$, 97-99%), L-alanine ($^{13}C3$, 99%), glycine (2-^{13}C, 99%; ^{15}N, 98%+), L-phenylalanine (D_8, 98%), or tyramine:HCl (1,1,2,2-D_4, 98%) (Cambridge Isotope Laboratories, Inc.) was added to BHIS containing 0.1% (w/v) deoxycholic acid (DCA) (Fisher Scientific). Control samples contained either no isotopically labeled amines, no DCA, or BHIS media without any additional supplement. Culture supernatants were prepared for metabolomic analysis as described above.

Metabolite analysis using GC-EI-MS with methoxyamine and TMS derivatization

Amine-containing metabolites were measured using GCMS with Electron Impact Ionization. Bacterial cultures were extracted using four volumes of 100% methanol. Following brief vortexing and centrifugation at 4°C, 20,000 x g for 15 min, 100 µL of extract supernatant was added to prelabeled mass spec autosampler vials (Microliter; 09-1200) and dried down completely under nitrogen stream at 30 L/min (top) 1 L/min (bottom) at 30°C (Biotage SPE Dry 96 Dual; 3579M). To dried samples, 50 µL of freshly prepared 20 mg/mL methoxyamine (Sigma; 226904) in pyridine (Sigma; 270970) was added and incubated in a thermomixer C (Eppendorf) for 90 min at 30°C and 1400 rpm. After samples are cooled to room temperature, 80 µL of derivatizing reagent (BSTFA + 1% TMCS; Sigma; B-023) and 70 µL of ethyl acetate (Sigma; 439169) were added and samples were incubated in a thermomixer at 70°C for 1 hour and 1400rpm. Samples were cooled to RT and 400 µL of Ethyl Acetate was added to dilute samples. Turbid samples were transferred to microcentrifuge tubes and centrifuged at 4°C, 20,000 x g for 15 min. Supernatants were then added to mass spec vials for GC-MS analysis. Samples were analyzed using a GC-MS

(Agilent 7890A GC system, Agilent 5975C MS detector) operating in electron impact ionization mode, using a HP-5MSUI column (30 m x 0.25 mm, 0.25 µm; Agilent Technologies 19091S-433UI) and 1 µL injection. Oven ramp parameters: 1 min hold at 60°C, 16° C per min up to 300° C with a 7 min hold at 300°C. Inlet temperature was 280° C and transfer line was 300° C. Data analysis was performed using MassHunter Quantitative Analysis software (version B.10, Agilent Technologies) and confirmed by comparison to authentic standards. Normalized peak areas were calculated by dividing raw peak areas of targeted analytes by averaged raw peak areas of $^{15}N,d_7$-L-proline and U-^{13}C-palmitate internal standards.

Bile acid analysis of human stool

Collection of pouchitis patient samples was approved by the Institutional Review Board of the University of Chicago. Patient 207 feces was liquid and extraction was performed by vortexing and diluting 1:2 (200 µL into 400 µL) with 100% methanol containing internal standards, followed by bath sonication for 10 minutes. Non-diseased volunteer donor feces were solid and were extracted by adding 80% methanol to 100 mg/mL and stored at −80 °C for at least one hour in beadruptor tubes (Fisherbrand; 15-340-154). Donor samples were then homogenized at 4 °C on a Bead Mill 24 Homogenizer (Fisher; 15-340-163) set at 1.6 m/s with six thirty-second cycles, five seconds off per cycle. All samples were then centrifuged at −10 °C, 20,000 x *g* for 15 min to generate supernatants for subsequent metabolomic analysis. Areas under the curve for culture supernatants were normalized to the average of D_4-taurocholate and D_4-taurodeoxycholate areas under the curve and multiplied by 1000, while areas under the curve for fecal samples were normalized to the average of D_4-taurocholate and D_4-glycocholate areas under the curve and multiplied by 1000.

All peak assignments in stool samples were verified by comparing the MS^2 fragmentation spectra to MS^2 fragmentation spectra established from the *in vitro* analyses described above.

B. fragilis P207 bile sensitivity growth assays

B. fragilis strain P207 was cultivated in BHIS supplemented with increasing concentrations of DCA, CA, GDCA, or GCA. Concentrations ranged from 0.024 mM to 6.17 mM of each compound. Strain P207 was grown from a saturated starter culture (~1.0 OD_{600}) that was back-diluted 1:100. Cultures were then grown for 24 hours, at which point terminal culture density was measured at OD_{600}.

Acknowledgements

We thank Doug Guzior for providing helpful references. Research reported in this publication was supported in part by the National Institutes of Health under award number 5RC2DK122394.

References

1. Russell DW. The enzymes, regulation, and genetics of bile acid synthesis. Annu Rev Biochem. 2003;72:137-74. doi: 10.1146/annurev.biochem.72.121801.161712.
2. Pellicoro A, van den Heuvel FA, Geuken M, Moshage H, Jansen PL, Faber KN. Human and rat bile acid-CoA:amino acid N-acyltransferase are liver-specific peroxisomal enzymes: implications for intracellular bile salt transport. Hepatology. 2007;45(2):340-8. doi: 10.1002/hep.21528.
3. Styles NA, Falany JL, Barnes S, Falany CN. Quantification and regulation of the subcellular distribution of bile acid coenzyme A:amino acid N-acyltransferase activity in rat liver. J Lipid Res. 2007;48(6):1305-15. doi: 10.1194/jlr.M600472-JLR200.
4. Heinken A, Ravcheev DA, Baldini F, Heirendt L, Fleming RMT, Thiele I. Systematic assessment of secondary bile acid metabolism in gut microbes reveals distinct metabolic capabilities in inflammatory bowel disease. Microbiome. 2019;7(1):75. doi: 10.1186/s40168-019-0689-3.
5. Ridlon JM, Kang DJ, Hylemon PB, Bajaj JS. Bile acids and the gut microbiome. Curr Opin Gastroenterol. 2014;30(3):332-8. doi: 10.1097/MOG.0000000000000057.
6. Hofmann AF. The Continuing Importance of Bile Acids in Liver and Intestinal Disease. Arch Intern Med. 1999;159(22):2647-58. doi: 10.1001/archinte.159.22.2647.
7. Guzior DV, Quinn RA. Review: microbial transformations of human bile acids. Microbiome. 2021;9(1):140. doi: 10.1186/s40168-021-01101-1.
8. Lucas LN, Barrett K, Kerby RL, Zhang Q, Cattaneo LE, Stevenson D, et al. Dominant Bacterial Phyla from the Human Gut Show Widespread Ability To Transform and Conjugate Bile Acids. mSystems. 2021:e0080521. doi: 10.1128/mSystems.00805-21.
9. Quinn RA, Melnik AV, Vrbanac A, Fu T, Patras KA, Christy MP, et al. Global chemical effects of the microbiome include new bile-acid conjugations. Nature. 2020;579(7797):123-9. doi: 10.1038/s41586-020-2047-9.
10. Copple BL, Li T. Pharmacology of bile acid receptors: Evolution of bile acids from simple detergents to complex signaling molecules. Pharmacol Res. 2016;104:9-21. doi: 10.1016/j.phrs.2015.12.007.
11. Kawamata Y, Fujii R, Hosoya M, Harada M, Yoshida H, Miwa M, et al. A G protein-coupled receptor responsive to bile acids. J Biol Chem. 2003;278(11):9435-40. doi: 10.1074/jbc.M209706200.
12. Sinha SR, Haileselassie Y, Nguyen LP, Tropini C, Wang M, Becker LS, et al. Dysbiosis-Induced Secondary Bile Acid Deficiency Promotes Intestinal Inflammation. Cell host & microbe. 2020;27(4):659-70.e5. doi: 10.1016/j.chom.2020.01.021.
13. Vineis JH, Ringus DL, Morrison HG, Delmont TO, Dalal S, Raffals LH, et al. Patient-Specific Bacteroides Genome Variants in Pouchitis. mBio. 2016;7(6). doi: 10.1128/mBio.01713-16.
14. Quillin SJ, Tran P, Prindle A. Potential Roles for Gamma-Aminobutyric Acid Signaling in Bacterial Communities. Bioelectricity. 2021;3(2):120-5. doi: 10.1089/bioe.2021.0012.
15. Marcobal A, De las Rivas B, Landete JM, Tabera L, Munoz R. Tyramine and phenylethylamine biosynthesis by food bacteria. Crit Rev Food Sci Nutr. 2012;52(5):448-67. doi: 10.1080/10408398.2010.500545.
16. Otaru N, Ye K, Mujezinovic D, Berchtold L, Constancias F, Cornejo FA, et al. GABA Production by Human Intestinal Bacteroides spp.: Prevalence, Regulation, and Role in Acid Stress Tolerance. Front Microbiol. 2021;12:656895. doi: 10.3389/fmicb.2021.656895.
17. Fiebig A, Schnizlein M, Pena-Rivera S, Trigodet F, Dubey AA, Hennessy M, et al. Multi-omics analysis of a Bacteroides fragilis isolate from an ulcerative colitis patient defines genetic determinants of fitness in bile. bioRxiv. 2023. doi: 10.1101/2023.05.11.540287.
18. Sinha SR, Haileselassie Y, Nguyen LP, Tropini C, Wang M, Becker LS, et al. Dysbiosis-Induced Secondary Bile Acid Deficiency Promotes Intestinal Inflammation. Cell host & microbe. 2020;27(4):659-70 e5. doi: 10.1016/j.chom.2020.01.021.
19. Lu S, Wang J, Chitsaz F, Derbyshire MK, Geer RC, Gonzales NR, et al. CDD/SPARCLE: the conserved domain database in 2020. Nucleic Acids Res. 2020;48(D1):D265-D8. doi: 10.1093/nar/gkz991.
20. Guzior D, Okros M, Martin Hernandez C, Shivel M, Armwald B, Hausinger R, et al. Bile salt hydrolase/aminoacyltransferase shapes the microbiome. 2022. doi: https://doi.org/10.21203/rs.3.rs-2050406/v1.
21. Patterson A, Rimal B, Collins S, Granda M, Koo I, Solanka S, et al. Bile Acids Are Substrates for Amine N-Acyl Transferase Activity by Bile Salt Hydrolase. 2022. doi: https://doi.org/10.21203/rs.3.rs-2050120/v1.
22. Ridlon JM, Kang DJ, Hylemon PB. Bile salt biotransformations by human intestinal bacteria. J Lipid Res. 2006;47(2):241-59. doi: 10.1194/jlr.R500013-JLR200.

23. Yao L, Seaton SC, Ndousse-Fetter S, Adhikari AA, DiBenedetto N, Mina AI, et al. A selective gut bacterial bile salt hydrolase alters host metabolism. Elife. 2018;7. doi: 10.7554/eLife.37182.
24. Alcantara C, Blasco A, Zuniga M, Monedero V. Accumulation of polyphosphate in Lactobacillus spp. and its involvement in stress resistance. Appl Environ Microbiol. 2014;80(5):1650-9. doi: 10.1128/AEM.03997-13.
25. Foley MH, Walker ME, Stewart AK, O'Flaherty S, Gentry EC, Patel S, et al. Bile salt hydrolases shape the bile acid landscape and restrict Clostridioides difficile growth in the murine gut. Nat Microbiol. 2023;8(4):611-28. doi: 10.1038/s41564-023-01337-7.
26. Sorg JA, Sonenshein AL. Bile salts and glycine as cogerminants for *Clostridium difficile* spores. J Bacteriol. 2008;190(7):2505-12. doi: 10.1128/jb.01765-07.
27. Theriot CM, Bowman AA, Young VB. Antibiotic-Induced Alterations of the Gut Microbiota Alter Secondary Bile Acid Production and Allow for Clostridium difficile Spore Germination and Outgrowth in the Large Intestine. mSphere. 2016;1(1). doi: 10.1128/mSphere.00045-15.
28. Floch MH, Binder HJ, Filburn B, Gershengoren W. The effect of bile acids on intestinal microflora. Am J Clin Nutr. 1972;25(12):1418-26. doi: 10.1093/ajcn/25.12.1418.
29. Hyland NP, Cryan JF. A Gut Feeling about GABA: Focus on GABA(B) Receptors. Front Pharmacol. 2010;1:124. doi: 10.3389/fphar.2010.00124.
30. Horvath TD, Ihekweazu FD, Haidacher SJ, Ruan W, Engevik KA, Fultz R, et al. Bacteroides ovatus colonization influences the abundance of intestinal short chain fatty acids and neurotransmitters. iScience. 2022;25(5):104158. doi: 10.1016/j.isci.2022.104158.
31. Brown C, Taniguchi G, Yip K. The monoamine oxidase inhibitor-tyramine interaction. J Clin Pharmacol. 1989;29(6):529-32. doi: 10.1002/j.1552-4604.1989.tb03376.x.
32. Kidd M, Modlin IM, Gustafsson BI, Drozdov I, Hauso O, Pfragner R. Luminal regulation of normal and neoplastic human EC cell serotonin release is mediated by bile salts, amines, tastants, and olfactants. Am J Physiol Gastrointest Liver Physiol. 2008;295(2):G260-72. doi: 10.1152/ajpgi.00056.2008.
33. Sun L, Zhang Y, Cai J, Rimal B, Rocha ER, Coleman JP, et al. Bile salt hydrolase in non-enterotoxigenic Bacteroides potentiates colorectal cancer. Nat Commun. 2023;14(1):755. doi: 10.1038/s41467-023-36089-9.
34. Pluskal T, Castillo S, Villar-Briones A, Oresic M. MZmine 2: modular framework for processing, visualizing, and analyzing mass spectrometry-based molecular profile data. BMC Bioinformatics. 2010;11:395. doi: 10.1186/1471-2105-11-395.
35. Nothias LF, Petras D, Schmid R, Duhrkop K, Rainer J, Sarvepalli A, et al. Feature-based molecular networking in the GNPS analysis environment. Nat Methods. 2020;17(9):905-8. doi: 10.1038/s41592-020-0933-6.
36. Wang M, Carver JJ, Phelan VV, Sanchez LM, Garg N, Peng Y, et al. Sharing and community curation of mass spectrometry data with Global Natural Products Social Molecular Networking. Nat Biotechnol. 2016;34(8):828-37. doi: 10.1038/nbt.3597.
37. Wang M, Jarmusch AK, Vargas F, Aksenov AA, Gauglitz JM, Weldon K, et al. Mass spectrometry searches using MASST. Nat Biotechnol. 2020;38(1):23-6. doi: 10.1038/s41587-019-0375-9.
38. Zhu QF, Wang YZ, An N, Hao JD, Mei PC, Bai YL, et al. Alternating Dual-Collision Energy Scanning Mass Spectrometry Approach: Discovery of Novel Microbial Bile-Acid Conjugates. Anal Chem. 2022;94(5):2655-64. doi: 10.1021/acs.analchem.1c05272.
39. de Hoon MJ, Imoto S, Nolan J, Miyano S. Open source clustering software. Bioinformatics. 2004;20(9):1453-4. doi: 10.1093/bioinformatics/bth078.

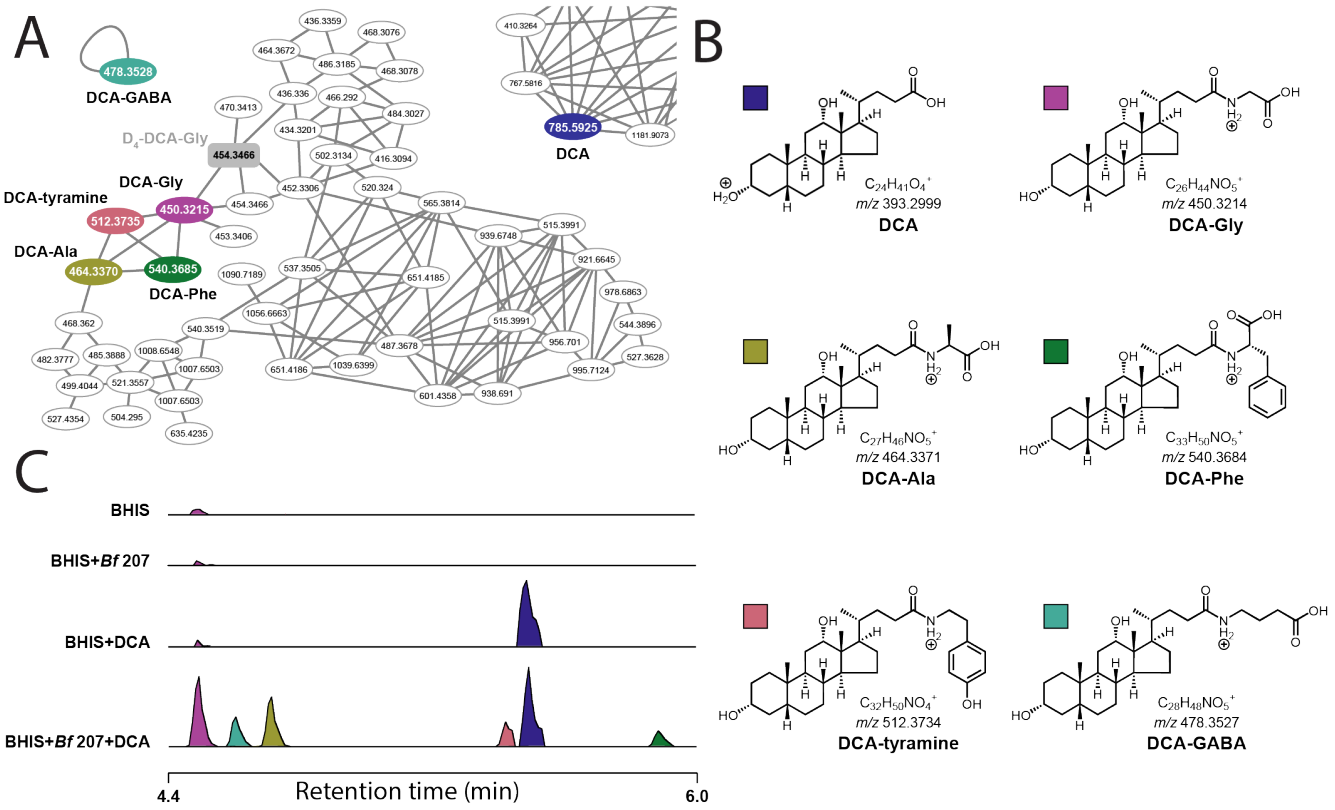

Figure 1. Identification of bile acid conjugates produced by pouchitis patient isolate, *B. fragilis* P207 by UHPLC-MS^2 (**A)** Molecular family containing nodes for deoxycholic acid (DCA)-amine conjugates. Colored nodes represent features only observed in *B. fragilis* P207 cultures with 0.01% (w/v) deoxycholic acid (DCA) present. The gray-shaded rectangular node is the D_4-DCA-Gly internal standard. **(B)** Structures of the five DCA-amines conjugates with color key for panels A, B, and C. (**C)** Stacked selected ion chromatograms for the five DCA-amino acid conjugates detected in BHIS media (BHIS), *B. fragilis* strain P207 culture extract (BHIS+*Bf* 207), BHIS media with 0.01% DCA (BHIS+DCA), and *B. fragilis* strain P207 culture extract with DCA (BHIS+*Bf* 207+DCA).

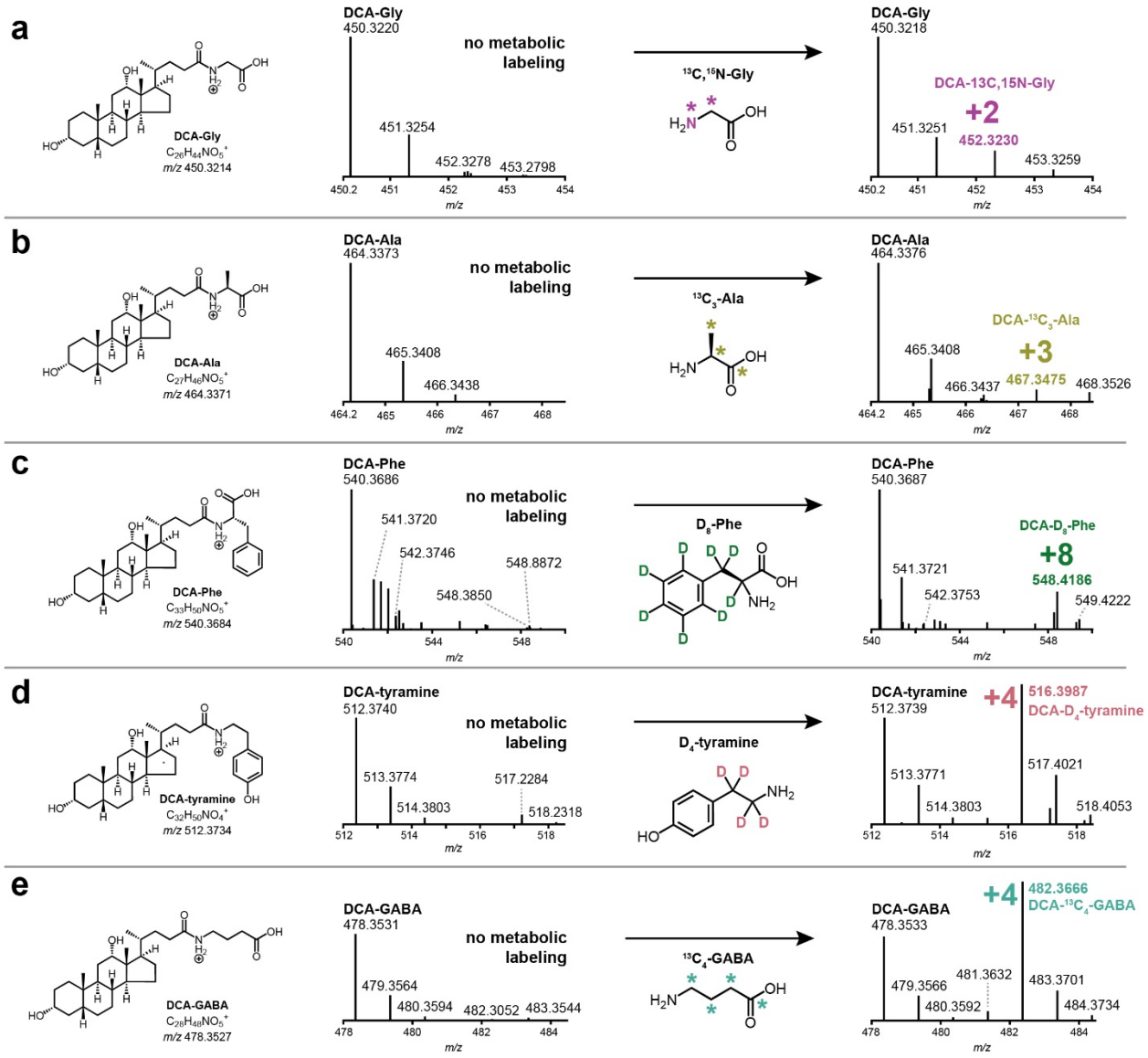

Figure 2. Amine feeding experiments confirming bile acid conjugation by *B. fragilis* strain P207. Mass spectrometry analysis was performed to assess production of bile acid conjugates with five different amines: glycine (a), alanine (b), phenylalanine (c), tyramine (d), and GABA (e). *B. fragilis* P207 was fed isotopically labeled versions of these amines. Observed mass shifts, displayed in each panel, are consistent with the expected molecular weights for the respective bile acid-heavy amino acid/amine conjugates presented in Figure 1.

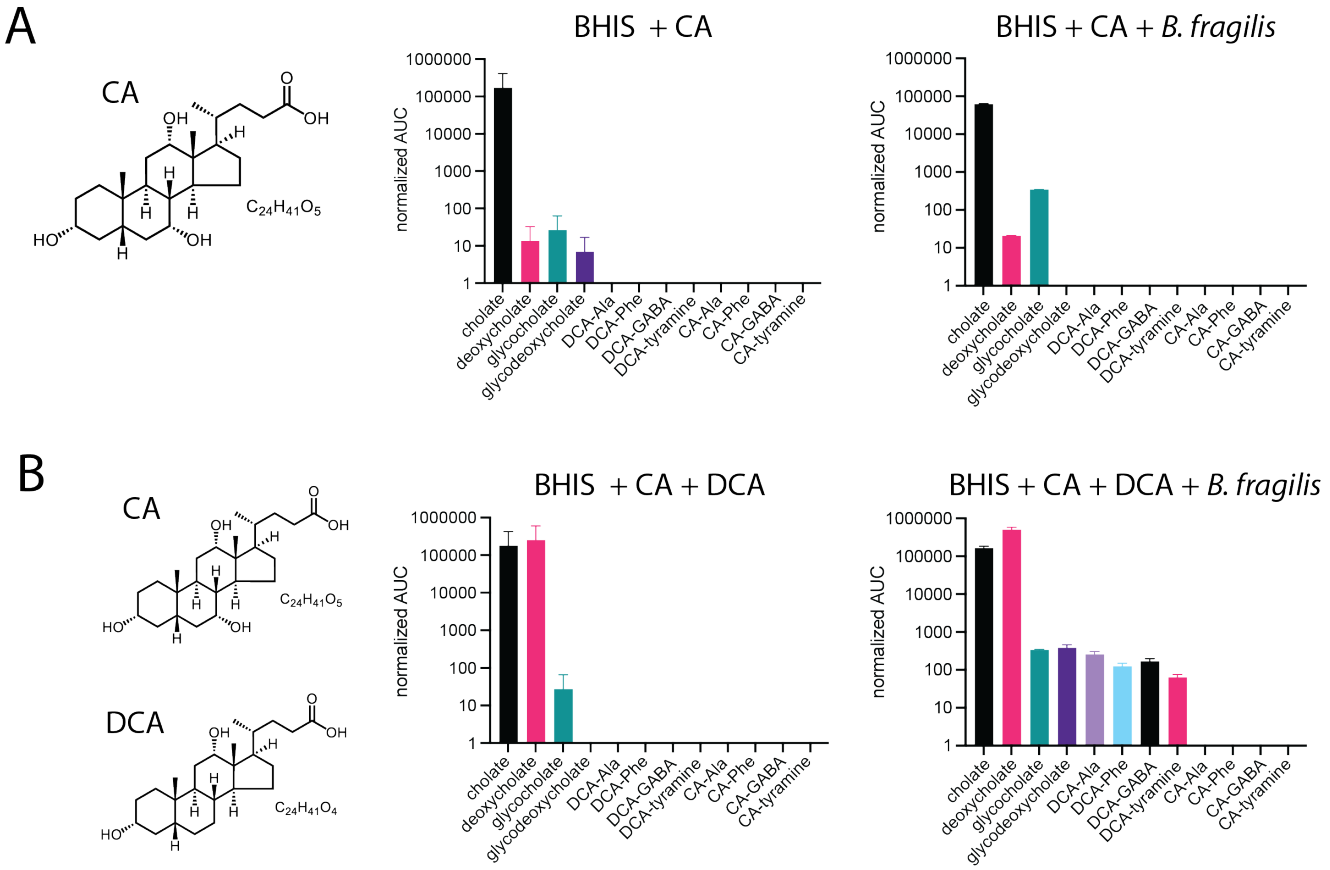

Figure 3. LC-MS/MS measurements of amino acid/amine conjugation to the bile acids cholic acid (CA) and deoxycholic acid (DCA) by *B. fragilis* P207. The bar graphs in this figure represent the mean area under the curve (AUC) of LC-MS/MS peaks corresponding to unconjugated or conjugated CA and DCA. (A) AUC of bile acid conjugate peaks (labeled below each bar) when *B. fragilis* P207 was cultivated in BHIS broth the presence of 0.01% (w/v) CA. (B) AUC of bile acid conjugate peaks when *B. fragilis* P207 was cultivated in BHIS broth the presence of CA and DCA (0.01% (w/v) total). The chemical structures of CA and DCA are provided on the left of each panel. Data represent the mean ± SD of three independent cultures.

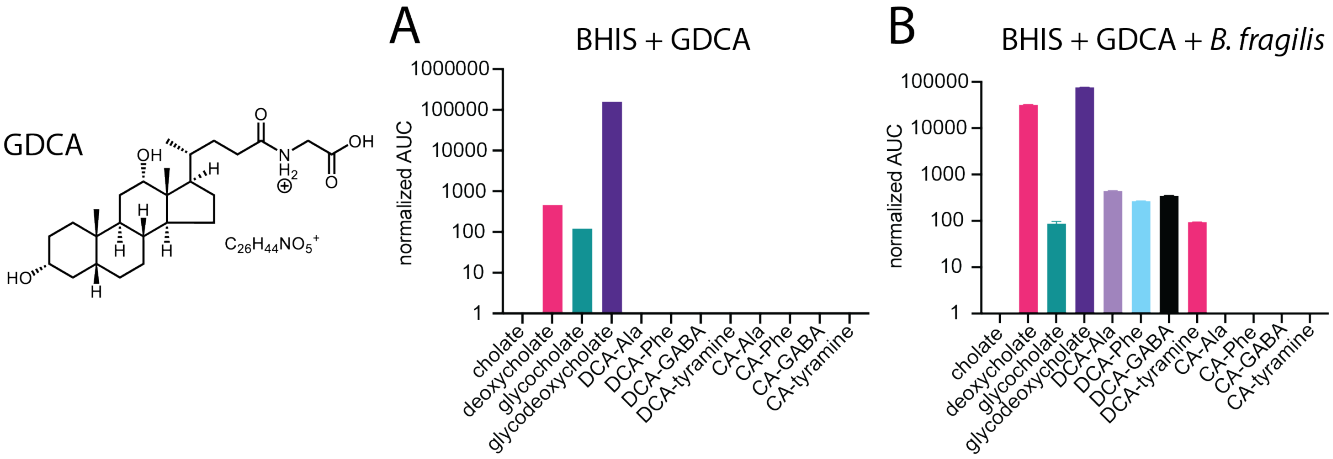

Figure 4. Production of deoxycholate (DCA) conjugates by *B. fragilis* P207 when provided with glycodeoxycholate (GDCA) as an initial substrate. Bars represent the mean area under the curve (AUC) of LC-MS/MS peaks. (A) AUC of bile acid peaks, labeled below each bar, of BHIS broth with 0.01% (w/v) GDCA added. Cholate and deoxycholate are known contaminants of the GDCA reagent (B) AUC of bile acid and bile acid conjugate peaks from *B. fragilis* P207 culture extract cultivated in BHIS broth the presence of 0.01% (w/v) GDCA. The chemical structure of GDCA is provided on the left of the panels. The absence of a bar indicates that a peak corresponding to that chemical species was not detected.

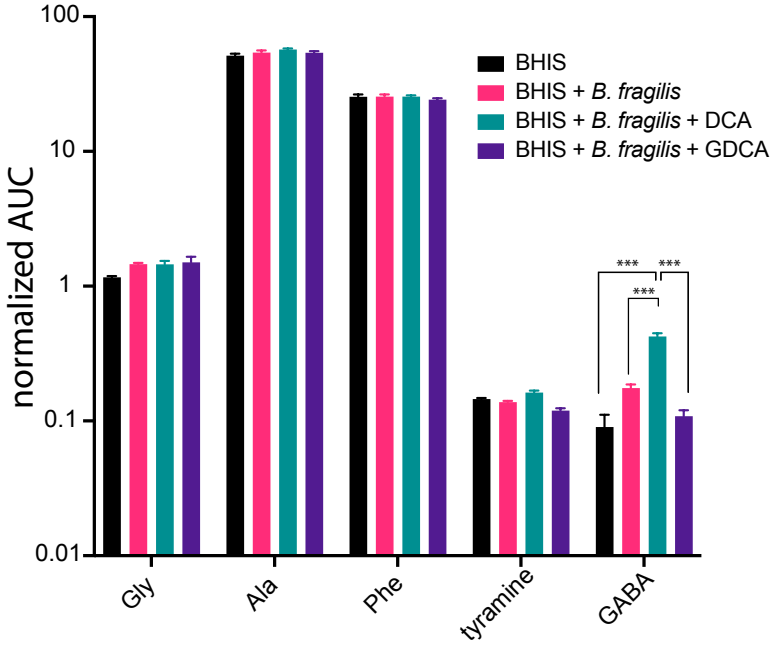

Figure 5: GC/MS-based detection of tyramine, glycine, alanine, phenylalanine, and GABA in *B. fragilis* P207 cultures. Cultures were grown in BHIS medium, both in the absence and presence of bile acids, DCA, and GDCA (0.01%, w/v). The displayed values, derived from the area under the curve (AUC) of detected peaks, represent the relative concentrations of these amine compounds across the different cultures. Each bar represents the mean of three independent experiments, with error bars indicating the standard deviations. Differences between conditions were assessed for statistical significance using ANOVA with Bonferroni correction. A threshold of $p < 0.001$ was considered to indicate statistical significance, ***.

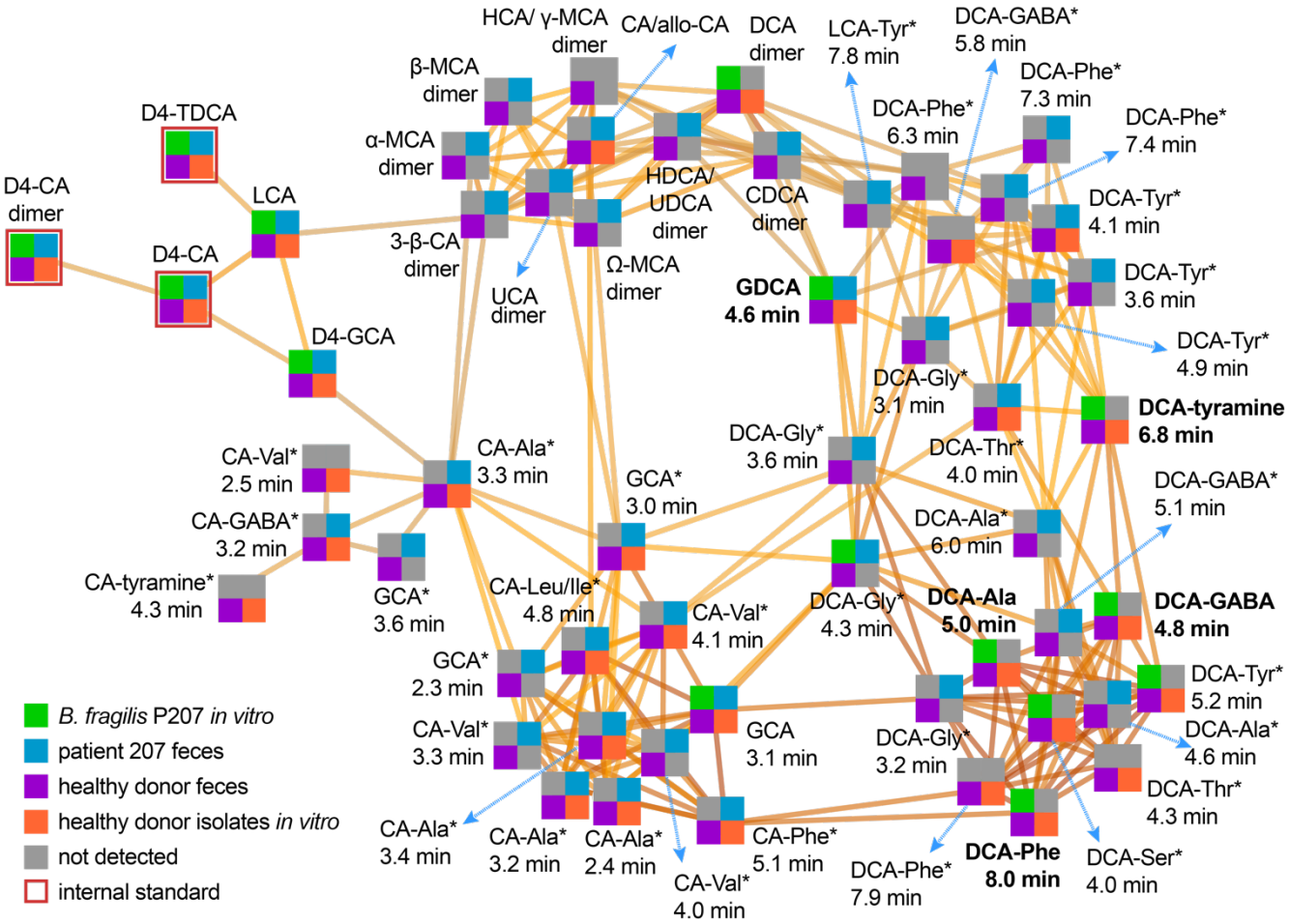

Figure 6. Molecular network illustrating the diversity and occurrence of bile acid-amine conjugates related to the validated DCA-Phe, DCA-Ala, DCA-Gly, DCA-tyramine, and DCA-GABA products. Each node represents a high-resolution *m/z* value at a specific retention time. Node quadrant color indicates the sample type that the metabolite was detected in—gray color indicates that the metabolite was not detected in the sample type specified by that quadrant. Edges connect nodes that are related above a score threshold of 25 in Compound Discoverer software suite (Thermo Scientific), with darker edges signifying greater relatedness. Bolded node labels indicate metabolites validated by isotope label experiments. Labels with an asterisk (*) indicate that the node represents a putative bile acid-amine isomer of the listed metabolite. These isomer assignments are based on comparison of *m/z* of the intact ion and MS^2 fragmentation spectra and fragment *m/z* values to the spectra of the validated bile acid conjugates. All other metabolite nodes were confirmed by comparison to authenticated standards or labeled internal standards.

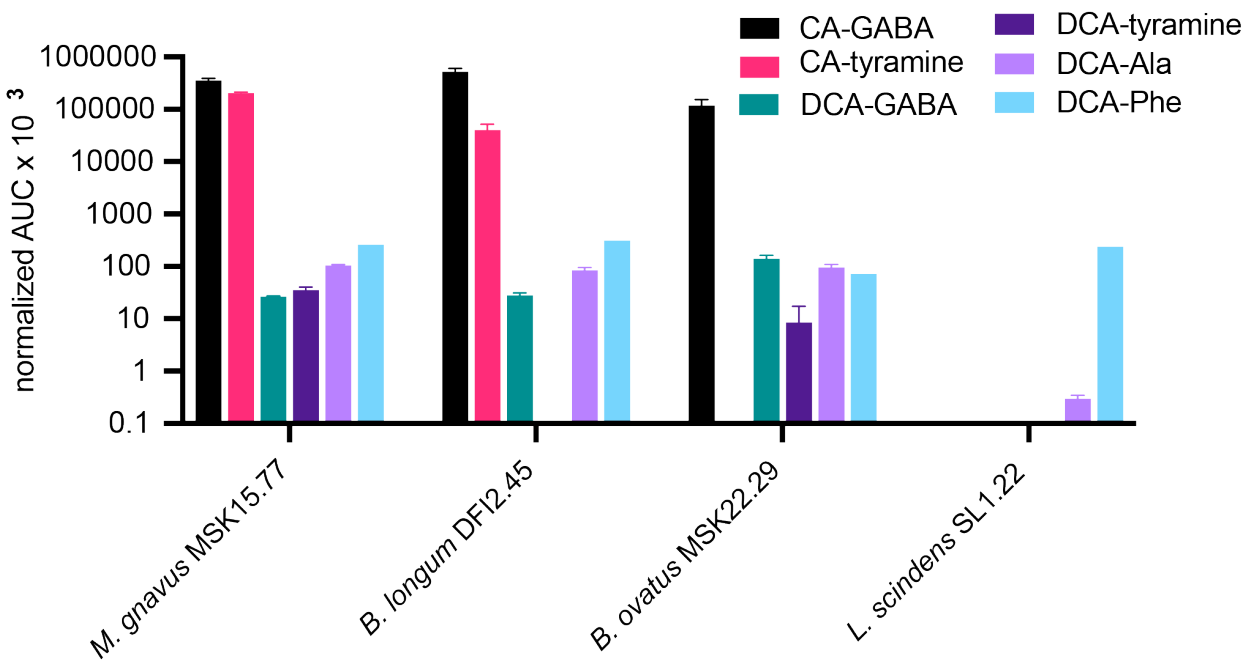

Figure 7. LC-MS/MS measurements of amino acid/amine conjugation to the bile acids cholic acid (CA) and deoxycholic acid (DCA) by *M. gnavus*, *B. longum*, *B. ovatus*, and *L. scidens* strains isolated from health human patients. The bar graphs in this figure represent the mean area under the curve (AUC) of LC-MS/MS peaks corresponding to unconjugated or conjugated CA and DCA. Normalized AUC of bile acid conjugate peaks (colored according to key) when strains were cultivated in BHIS broth the presence of 0.01% (w/v) DCA or CA. The absence of a bar indicates that a peak corresponding to that chemical species was not detected.

Supplemental Results

Microbially-catalyzed conjugation of GABA and tyramine to bile acids

Michael W. Mullowney[1], Aretha Fiebig[2], Matthew K. Schnizlein [2], Mary McMillin[1], Jason Koval[3], David Rubin[3], Sushila Dalal[3], Mitch Sogin[4], Eugene B. Chang[3], Ashley M. Sidebottom[1], Sean Crosson[2]

Mass spectrometry data

Glycine conjugate
Broth from P207 cultures containing DCA and unlabeled glycine or isotopically labeled glycine ($^{13}C_2$, 99%; ^{15}N, 98%+) revealed a DCA-Gly conjugate with an $[M+H]^+$ of *m/z* 450.3220 and a corresponding labeled ion with an $[M+H]^+$ of *m/z* 452.3230, respectively (Figure 2A). Analysis of tandem MS fragmentation indicated condensation of the amine of Gly with DCA at the terminal side-chain carboxylic acid (Figure S1). Key MS^2 fragments from unlabeled P207 culture samples that indicate the position of the glycine on DCA include the doubly dehydroxylated DCA-Gly conjugate ion (*m/z* 414.3007), the *N*-(1-Oxo-4-penten-1-yl)glycine ion (*m/z* 158.0807), and the glycine aminium ion (*m/z* 76.0393). Ions with two Dalton increases corresponding to these were observed in MS^2 data associated with an MS^1 scan with a two Dalton increase in the glycine ($^{13}C_2$, 99%; ^{15}N, 98%+) labeled sample, further confirming the structural assignment of glycine conjugation at the terminal side-chain carboxylic acid of DCA.

Alanine conjugate
Broth from strain P207 cultures containing DCA and unlabeled L-alanine or isotopically labeled L-alanine ($^{13}C_3$, 99%) revealed a DCA-Ala conjugate with an $[M+H]^+$ of *m/z* 464.3373 and a corresponding labeled ion with an $[M+H]^+$ of *m/z* 467.3475, respectively (Figure 2B). The tandem MS fragmentation profile indicated condensation of the amine of Ala with DCA at the terminal side-chain carboxylic acid (Figure S2). Key MS^2 fragments from unlabeled P207 cultures that support the position of the alanine on DCA include the doubly dehydroxylated DCA-Ala conjugate ion (*m/z* 428.3165), the *N*-(1-Oxo-4-penten-1-yl)alanine ion (*m/z* 172.0963), and the alanine aminium ion (*m/z* 90.0544). Ions with three Dalton increases corresponding to the dehydroxylated DCA-Ala conjugate and the alanine aminium ion were observed in MS^2 data associated with an MS^1 scan with a three Dalton increase in the L-alanine ($^{13}C_3$, 99%) sample. These results further support the structural assignment of alanine conjugation at the terminal side-chain carboxylic acid of DCA, which was recently described using an alternative derivatization method [38].

Phenylalanine conjugate
Comparison of broth from P207 cultures containing DCA and unlabeled L-phenylalanine or isotopically labeled L-phenylalanine (D_8, 98%) revealed a DCA-Phe conjugate with an $[M+H]^+$ of *m/z* 540.3684 and a corresponding labeled ion with an $[M+H]^+$ of *m/z* 548.4186, respectively (Figure 2C). Analysis of tandem MS fragmentation indicated condensation of the amine of Phe with DCA at the terminal side-chain carboxylic acid (Figure S3). Key MS^2 fragments that indicate the position of the phenylalanine on DCA include the doubly dehydroxylated DCA-Phe conjugate ion (*m/z* 504.3472), the *N*-(1-Oxo-4-penten-1-yl)phenylalanine ion (*m/z* 248.1281), the phenylalanine aminium ion (*m/z* 166.0861), and the phenylalanine iminium ion (*m/z* 120.0805). Ions corresponding to the doubly dehydroxylated DCA-Phe conjugate ion and the phenylalanine aminium and iminium ions with eight Dalton increases were observed in MS^2 data associated with an MS^1 scan with an eight Dalton increase in the L-phenylalanine (D_8, 98%) sample, further confirming the structural assignment of phenylalanine conjugation at the terminal side-chain carboxylic acid of DCA. Additionally, comparison of data from DCA-Phe in our study to that of phenylalanocholic acid (Phe-cholic acid) in Quinn, et al. [9] supports these results. Specifically, we observed matches between the phenylalanine ammonium and iminium ions as well as expected fragment shifts between the two MS^2 spectra arising from the absence of a hydroxyl group in DCA-Phe.

Tyramine conjugate
Comparison of broth from P207 cultures containing DCA and unlabeled tyramine or isotopically labeled tyramine:HCl (1,1,2,2-D_4, 98%) revealed a DCA-tyramine conjugate with an $[M+H]^+$ of *m/z* 512.3740 and a corresponding labeled ion with an $[M+H]^+$ of *m/z* 516.3987, respectively (Figure 2D). Analysis of tandem MS

fragmentation indicated condensation of the amine of tyramine with DCA at the terminal side-chain carboxylic acid (Figure S4). Key MS^2 fragments in data from the unlabeled P207 cultures that indicate the position of the tyramine on DCA include the doubly dehydroxylated DCA-tyramine conjugate ion (*m/z* 476.3526), the dehydroxylated DCA-tyramine conjugate ion (*m/z* 494.3629), the *N*-(1-Oxo-4-penten-1-yl)tyramine ion (*m/z* 220.1330), the tyramine cation (*m/z* 138.0913), and the 2-(4-hydroxyphenyl)ethylium ion (*m/z* 121.0644). Ions corresponding to these with four Dalton increases were observed in MS^2 data associated with an MS^1 scan with a four Dalton increase in the tyramine:HCl (1,1,2,2-D_4, 98%) sample, further confirming the structural assignment of tyramine conjugation at the terminal side-chain carboxylic acid of DCA to produce tyraminodeoxycholic acid.

GABA conjugate

More specifically, comparison of broth from P207 cultures containing DCA and unlabeled 4-aminobutyric acid (GABA) or isotopically labeled GABA ($^{13}C_4$, 97-99%) revealed a DCA-GABA conjugate with an $[M+H]^+$ of *m/z* 478.3531 and a corresponding labeled ion with an $[M+H]^+$ of *m/z* 482.3666, respectively (Figure 2E). Analysis of tandem MS fragmentation indicated condensation of the primary amine of GABA with DCA at the terminal side-chain carboxylic acid (Figure S5). Key MS^2 fragments in data from the unlabeled P207 cultures that indicate the position of GABA on DCA include the doubly dehydroxylated DCA-GABA conjugate ion (detected *m/z* 442.3316), the *N*-(1-Oxo-4-penten-1-yl)-GABA ion (detected *m/z* 186.1121), the GABA cation (detected *m/z* 104.0706), and the GABA iminium ion (detected *m/z* 86.0596). Samples from GABA ($^{13}C_4$, 97-99%)-labeled broth contained ions with four Dalton increases corresponding to each of these MS^2 fragments, which were associated with an MS^1 scan with a four Dalton increase. These results further support the structural assignment of GABA conjugation at the terminal side-chain carboxylic acid of DCA to produce γ-aminobutyrodeoxycholic acid.

Table S1. Possible DCA-AA conjugates with predicted positive and negative ions used to search raw mass spectrometry data and molecular networks.

DCA-AA conjugate	$[M+H]^+$	$[M-H]^-$
DCA-Urea	435.3218	433.3072
DCA-Glycine	450.3214	448.3068
DCA-Glycolic acid	451.3054	449.2908
DCA-Alanine	464.3371	462.3225
DCA-beta-Alanine	464.3371	462.3225
DCA-Sarcosine	464.3371	462.3225
DCA-Lactic acid	465.3211	463.3065
DCA-Glycerol	467.3367	465.3221
DCA-Phosphoric acid	473.2663	471.2517
DCA-GABA	478.3527	476.3381
DCA-Serine	480.3320	478.3174
DCA-Uracil	487.3167	485.3021
DCA-ornithine lactam	489.3687	487.3541
DCA-Proline	490.3527	488.3381
DCA-Fumarate	491.3004	489.2858
DCA-Valine	492.3684	490.3538
DCA-Succinic acid	493.3160	491.3014
DCA-Threonine	494.3476	492.3330
DCA-Cysteine	496.3092	494.2946
DCA-Nicotinamide	497.3374	495.3228
DCA-Taurine	500.3041	498.2895
DCA-5-oxoprolinate	504.3320	502.3174
DCA-5-oxoproline	504.3320	502.3174
DCA-L-Isoleucine	506.2894	504.2748
DCA-Leucine	506.3840	504.3694
DCA-Isoleucine	506.3840	504.3694
DCA-Asparagine	507.3429	505.3283
DCA-ornithine	507.3793	505.3647
DCA-Aspartic acid	508.3269	506.3123
DCA-Malate	509.3109	507.2963
DCA-Erythronic acid	511.3266	509.3120
DCA-Hypoxanthine	511.3279	509.3133
DCA-tyramine	512.3735	510.3589
DCA-2-Oxoglutarate	521.3109	519.2963
DCA-Glutamine	521.3585	519.3439
DCA-Lysine	521.3949	519.3803
DCA-Glutamic acid	522.3426	520.3280
DCA-Methionine	524.3405	522.3259
DCA-histidine	530.3589	528.3443
DCA-Phenylalanine	540.3684	538.3538
DCA-selenocysteine	543.2458	541.2312

DCA-Capric acid	547.4357	545.4211
DCA-argninine	549.4011	547.3865
DCA-N-Acetylaspartic acid	550.3375	548.3229
DCA-Tyrosine	556.3633	554.3487
DCA-Azelaic acid	563.3943	561.3797
DCA-N-Acetylglutamic acid	564.3531	562.3385
DCA-Citrate	567.3164	565.3018
DCA-Isocitrate	567.3164	565.3018
DCA-tryptophan	579.3793	577.3647
DCA-Pantothenic acid	594.3994	592.3848
DCA-Myristic acid	603.4983	601.4837
DCA-Palmitoleic acid	629.5140	627.4994
DCA-pyrolysine	630.4477	628.4331
DCA-Palmitic acid	631.5296	629.5150
DCA-Oleic acid	657.5453	655.5307
DCA-Stearic acid	659.5609	657.5463
DCA-Docosahexaenoic acid	703.5296	701.5150
DCA-Cholesterol	761.6443	759.6297
DCA-(2R)-Pyrrolidine	762.9894	760.9748

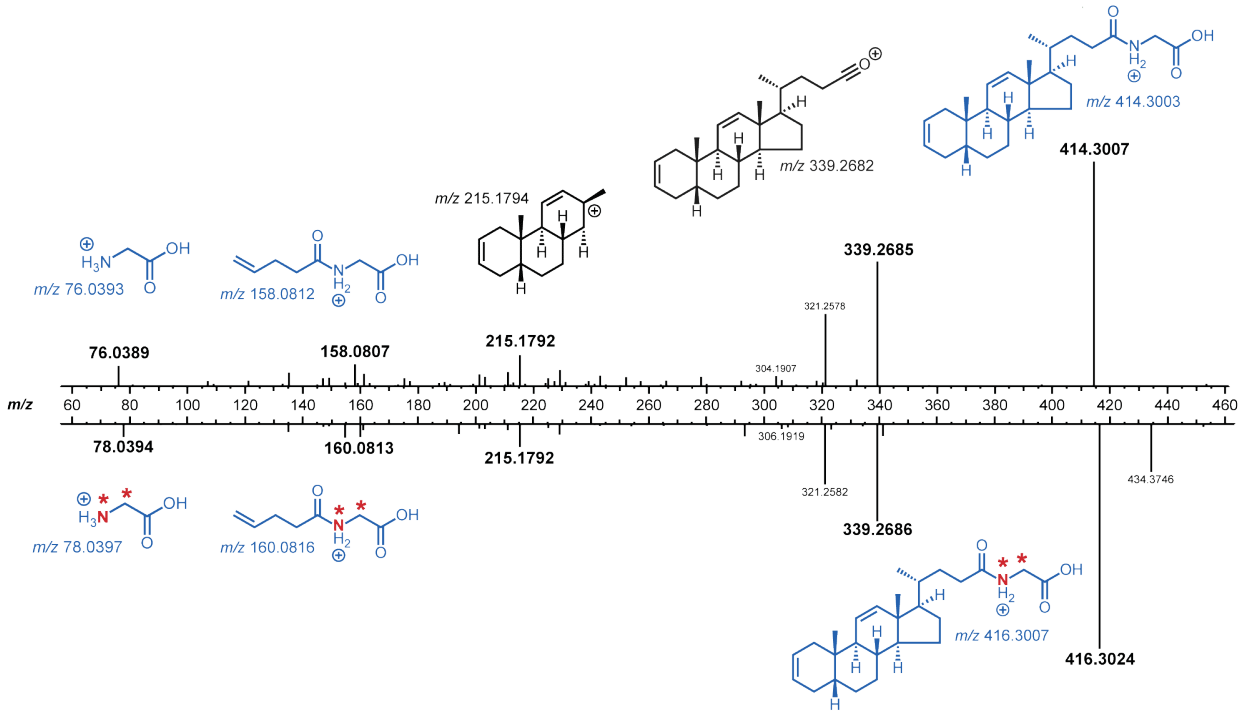

Figure S1. Mirror plot of a summed DCA-Gly (*m/z* 450.3220) MS^2 spectrum opposite a summed MS^2 spectrum for the isotopically labeled DCA-^{15}N,^{13}C-Gly (*m/z* 452.3230), which was observed only when *B. fragilis* P207 was cultured in the presence of DCA and ^{15}N,^{13}C-Gly (Figure 2). The +2 deuterium shift was observed in the expected MS^2 fragments between the spectra. (red asterisk indicating location of deuteriums). All structural assignments for MS2 ions are putative.

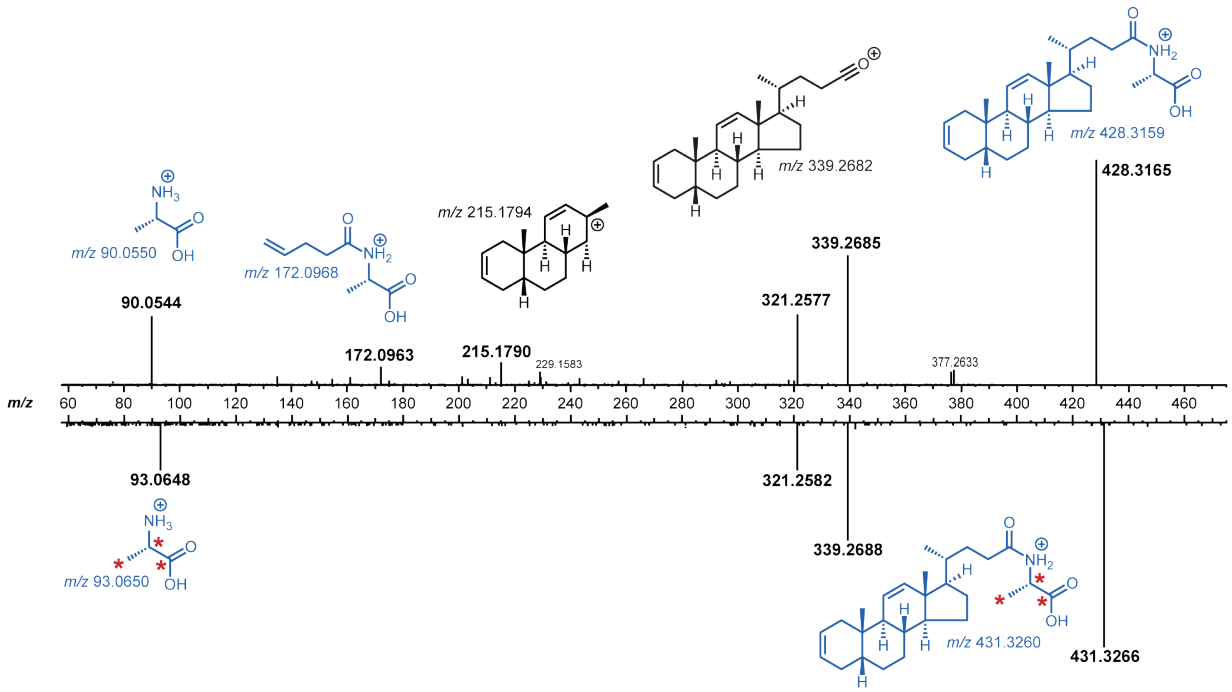

Figure S2. Mirror plot of a summed DCA-Ala (*m/z* 464.3373) MS^2 spectrum opposite a summed MS^2 spectrum for the isotopically labeled DCA-$^{13}C_3$-Ala (*m/z* 467.3475), which was observed only when *B. fragilis* P207 was cultured in the presence of DCA and $^{13}C_3$-Ala (Figure 2). The +3 deuterium shift was observed in the expected MS^2 fragments between the spectra (red asterisk indicating location of deuteriums). All structural assignments for MS2 ions are putative.

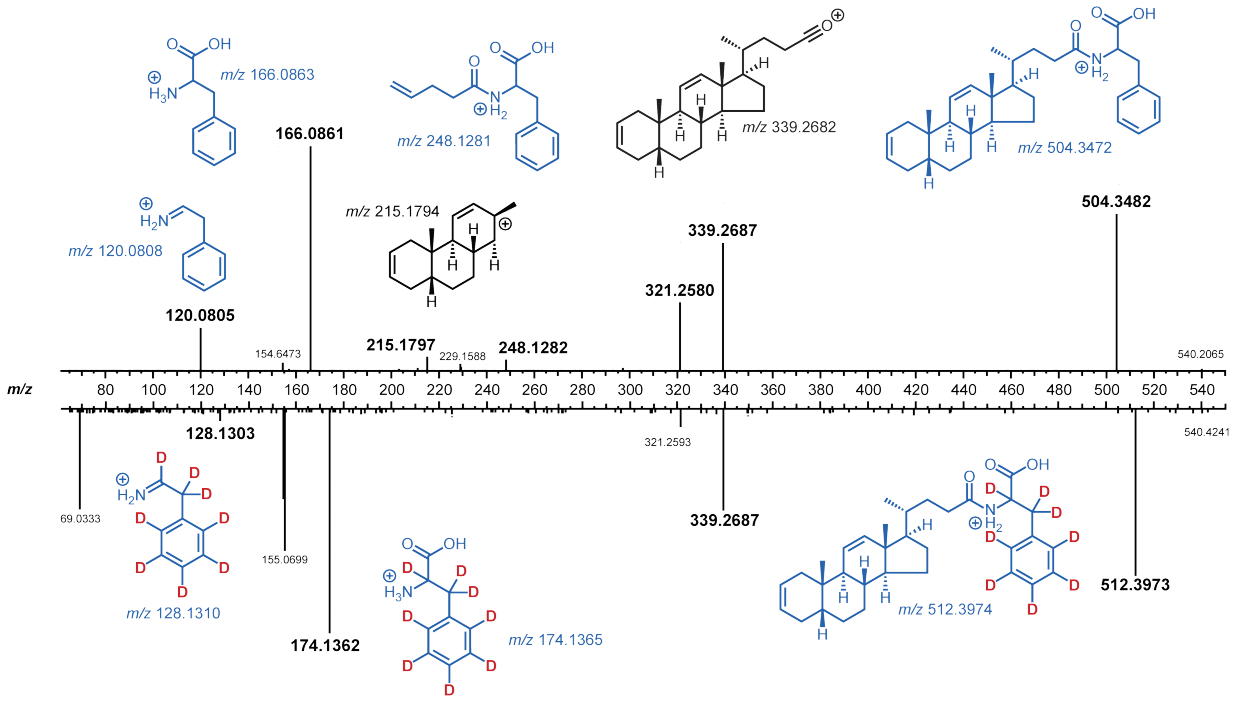

Figure S3. Mirror plot of a summed DCA-Phe (*m/z* 540.3686) MS^2 spectrum opposite a summed MS^2 spectrum for the isotopically labeled DCA-D_8-Phe (*m/z* 548.4186), which was observed only when *B. fragilis* P207 was cultured in the presence of DCA and D_8-Phe (Figure 2). The +8 deuterium shift was observed in the expected MS^2 fragments between the spectra (red text indicating location of deuteriums). All structural assignments for MS2 ions are putative.

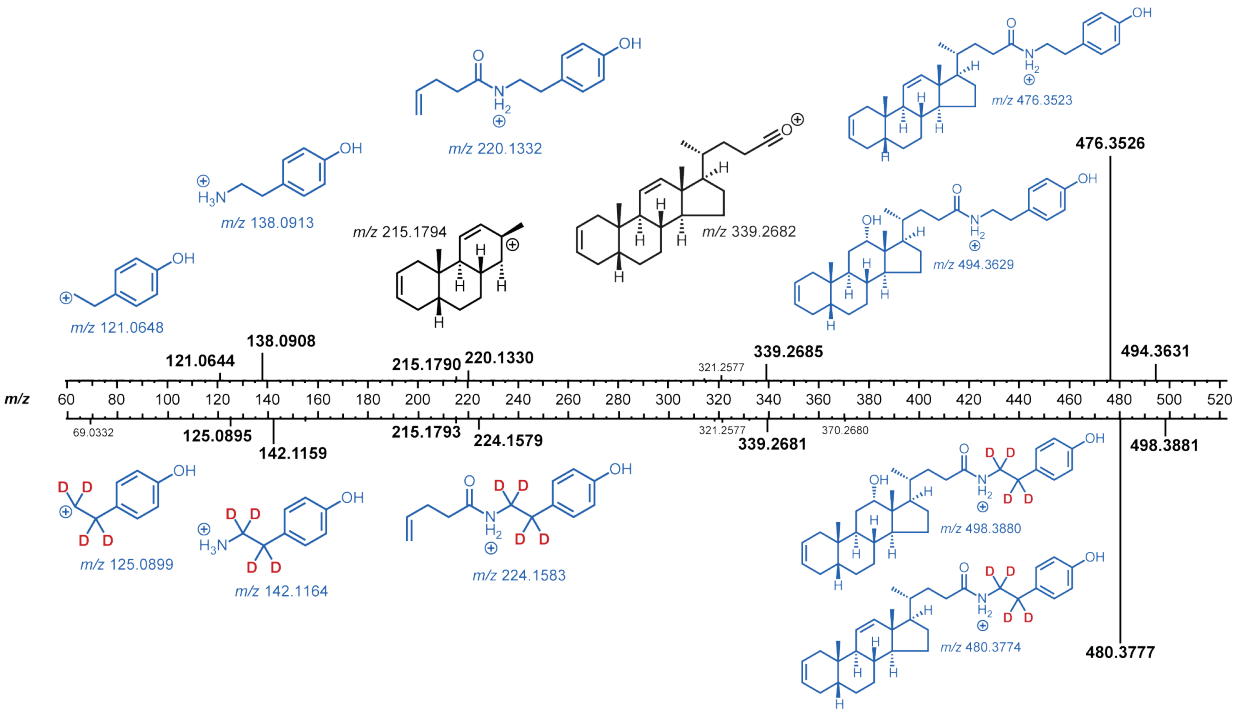

Figure S4. Mirror plot of a summed DCA-tyramine (*m/z* 512.3740) MS^2 spectrum opposite a summed MS^2 spectrum for the isotopically labeled DCA-D_4-tyramine (*m/z* 516.3987), which was observed only when *B. fragilis* P207 was cultured in the presence of DCA and D_4-tyramine (Figure 2). The +4 deuterium shift was observed in the expected MS^2 fragments between the spectra (red asterisk indicating location of deuteriums). All structural assignments for MS2 ions are putative.

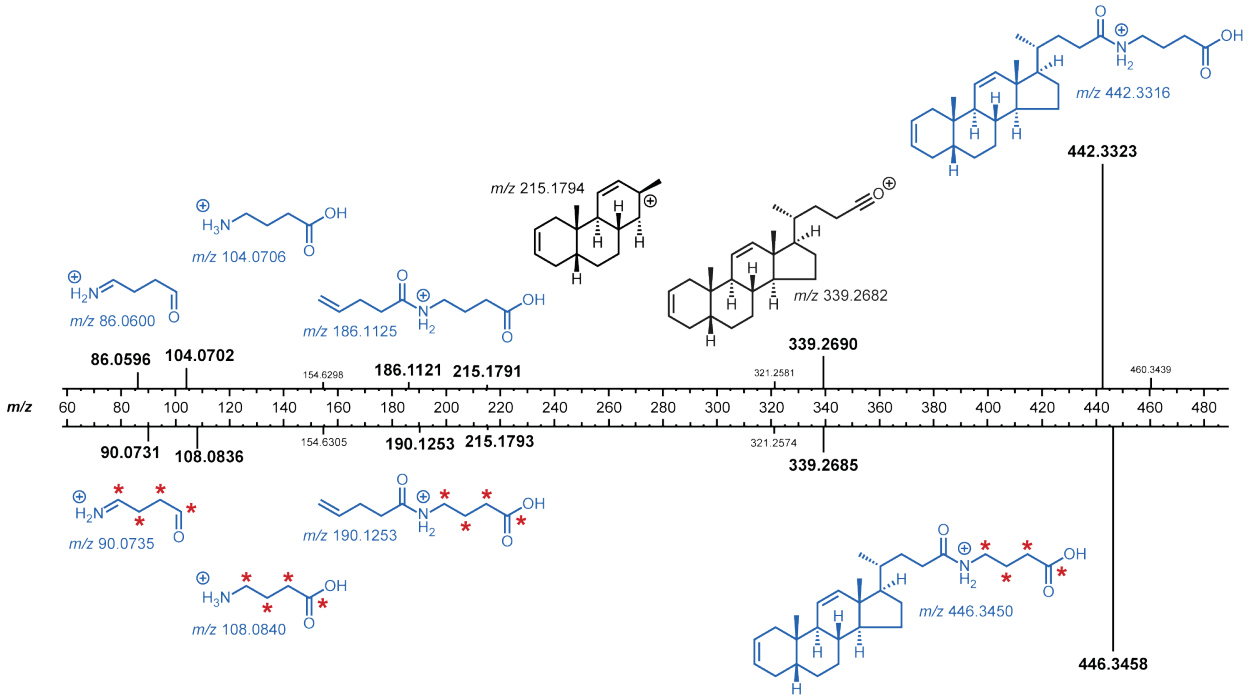

Figure S5. Mirror plot of a summed DCA-GABA (*m/z* 478.3531) MS^2 spectrum opposite a summed MS^2 spectrum for the isotopically labeled DCA-$^{13}C_4$-GABA (*m/z* 482.3666), which was observed only when *B. fragilis* P207 was cultured in the presence of DCA and $^{13}C_4$-GABA (Figure 2). The +4 deuterium shift was observed in the expected MS^2 fragments between the spectra (red asterisk indicating location of deuteriums). All structural assignments for MS2 ions are putative.

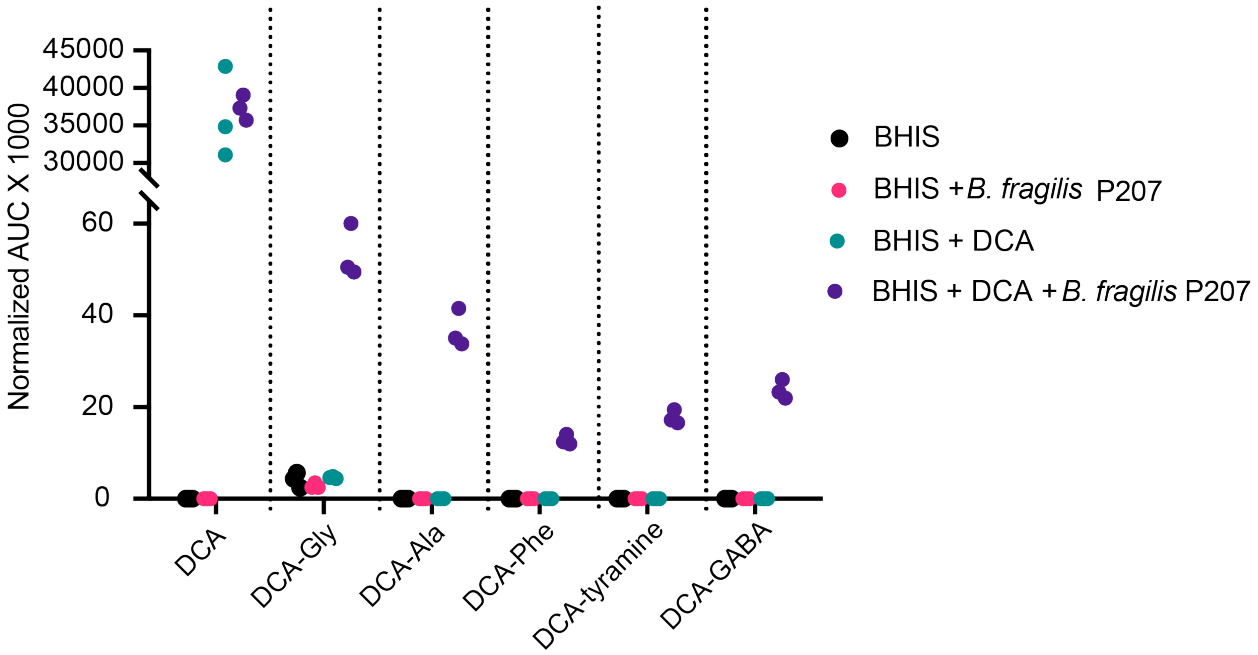

Figure S6. Relative abundances of the five deoxycholic acid (DCA)-amine conjugates in triplicate samples of BHIS media, BHIS media with *B. fragilis* strain P207 (P207), BHIS media with DCA, and BHIS media with P207 and DCA normalized to the average peak area under the curve (AUC) for internal standard ions D_4-taurocholic acid $[M+H]^+$ at *m/z* 520.3241, D_4-taurodeoxycholic acid $[M+H]^+$ at *m/z* 504.3291, and D_4-glycocholic acid at m/z 470.3414.

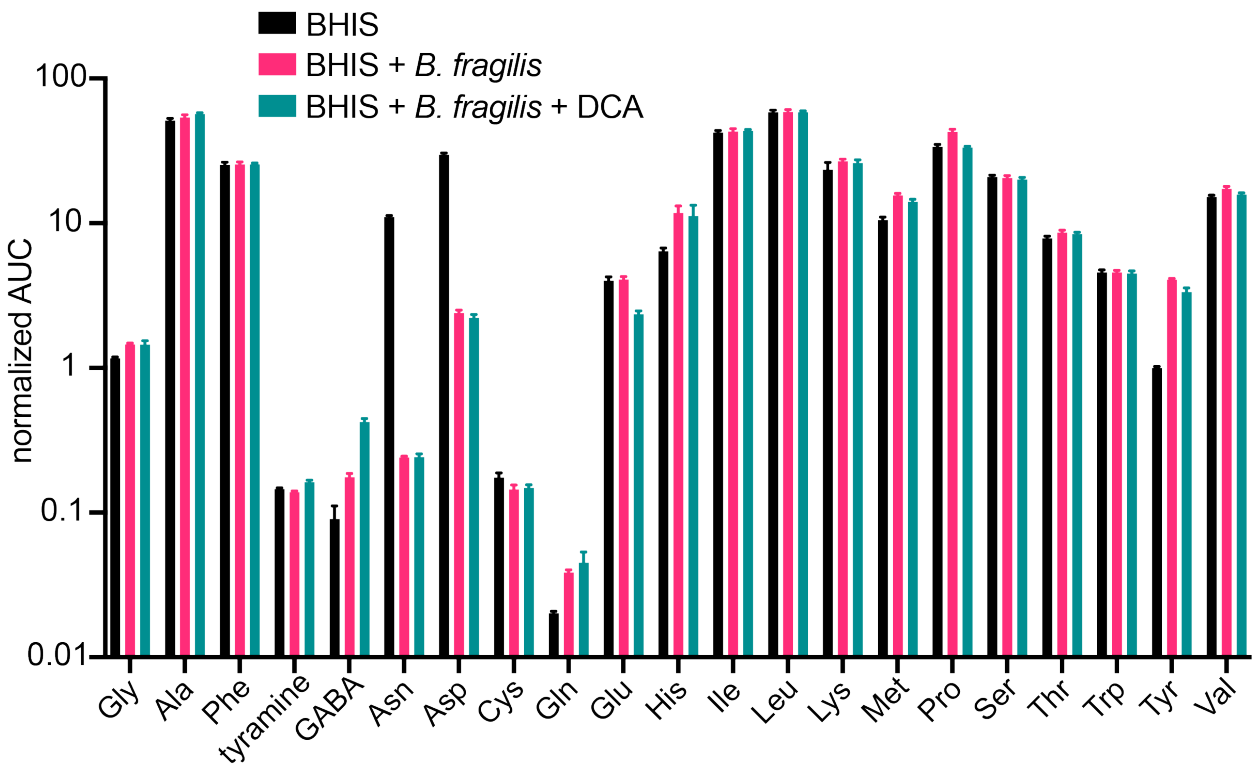

Figure S7. GC/MS-based measurement of select amines in *B. fragilis* P207 cultures. The cultures were grown in BHIS medium in the absence or presence of the bile acid, DCA (0.01%, w/v). The displayed values, derived from the area under the curve (AUC) of detected peaks, represent the relative concentrations of these compounds across the different cultures. Each bar represents the mean of three independent experiments, with error bars indicating the standard deviations.

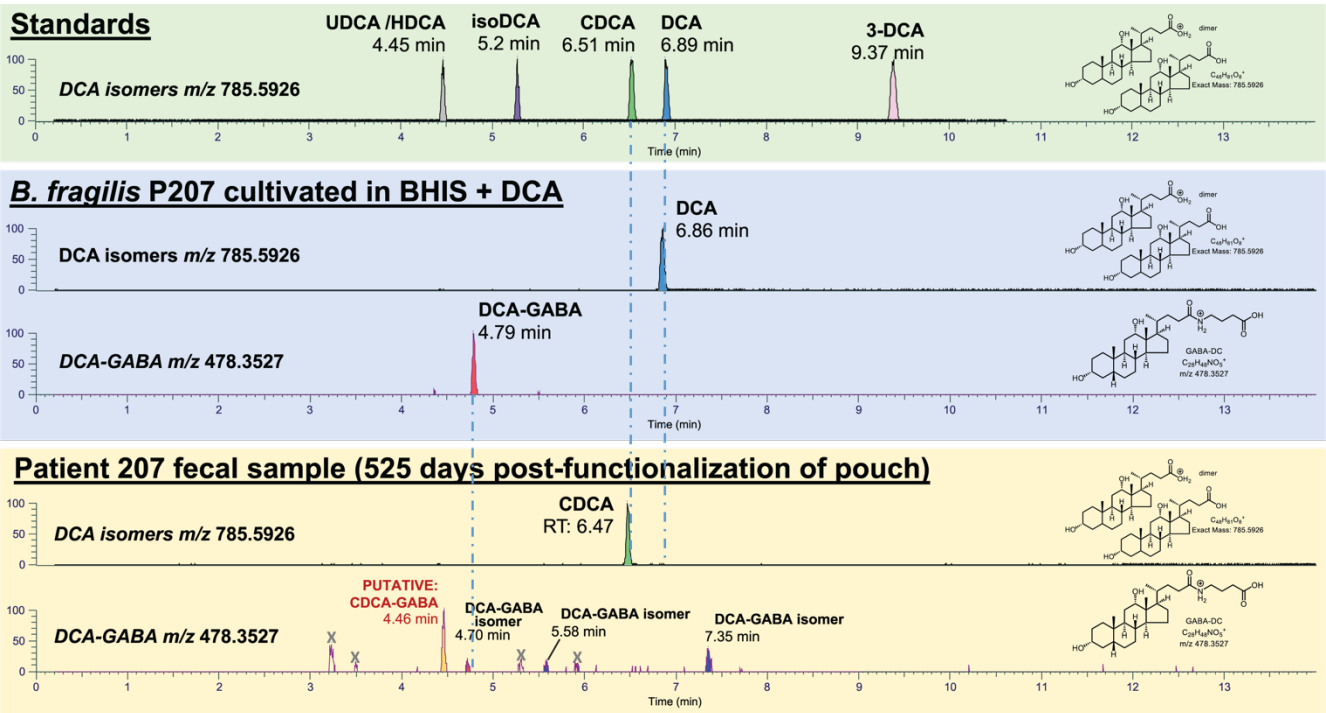

Figure S8. (Top panel) Liquid chromatography temporal elution profile of deoxycholic acid (DCA) and DCA isomer standards (*m/z* dimer 785.5926): ursodeoxycholic acid (UDCA); hyodeoxycholic acid (HDCA); chenodeoxycholic acid (CDCA). (Middle panel) Incubation of *B. fragilis* strain P207 with 0.01% (w/v) DCA in BHIS broth followed by LC separation of culture extract and MS/MS analysis provides evidence for production of DCA-GABA *in vitro*. Quantification of all five DCA conjugates detected in *B. fragilis* strain P207 culture extract by MS/MS are presented in Figure S6 and Table S2. (bottom panel) Fecal extract of pouchitis patient 207 across multiple time points yielded multiple peaks with MS/MS profiles matching GABA conjugated to DCA. The absence of DCA in patient 207 stool suggests these species are DCA isomer-GABA conjugates (labeled DCA-GABA isomer). Panel provides the profile at 525 days post functionalization of the J-pouch. Quantification of bile acid peaks across an approximate 2-year period are presented in Table S2.

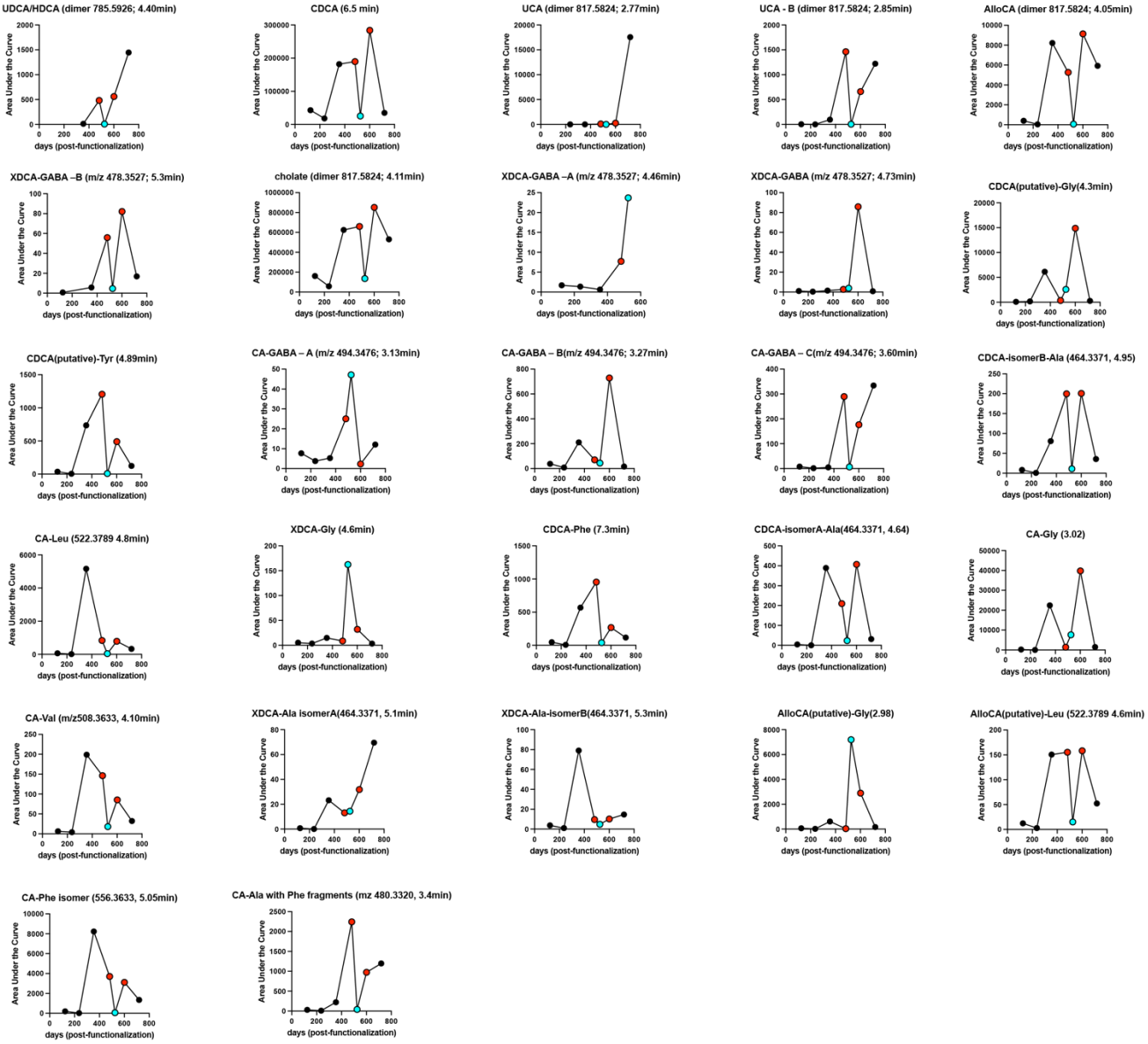

Figure S9. Temporal profile of unconjugated and conjugated bile acid species in pouchitis patient 207 from 124 to 719 days [13]. Red dots at 482 and 719 days post-functionalization are clinic visits in which the patient was determined to have pouch inflammation (i.e. pouchitis). Blue dot was during a period of antimicrobial treatment, in which the patient did not have pouchitis. The top of each graph notes the elution time of each species in minutes.

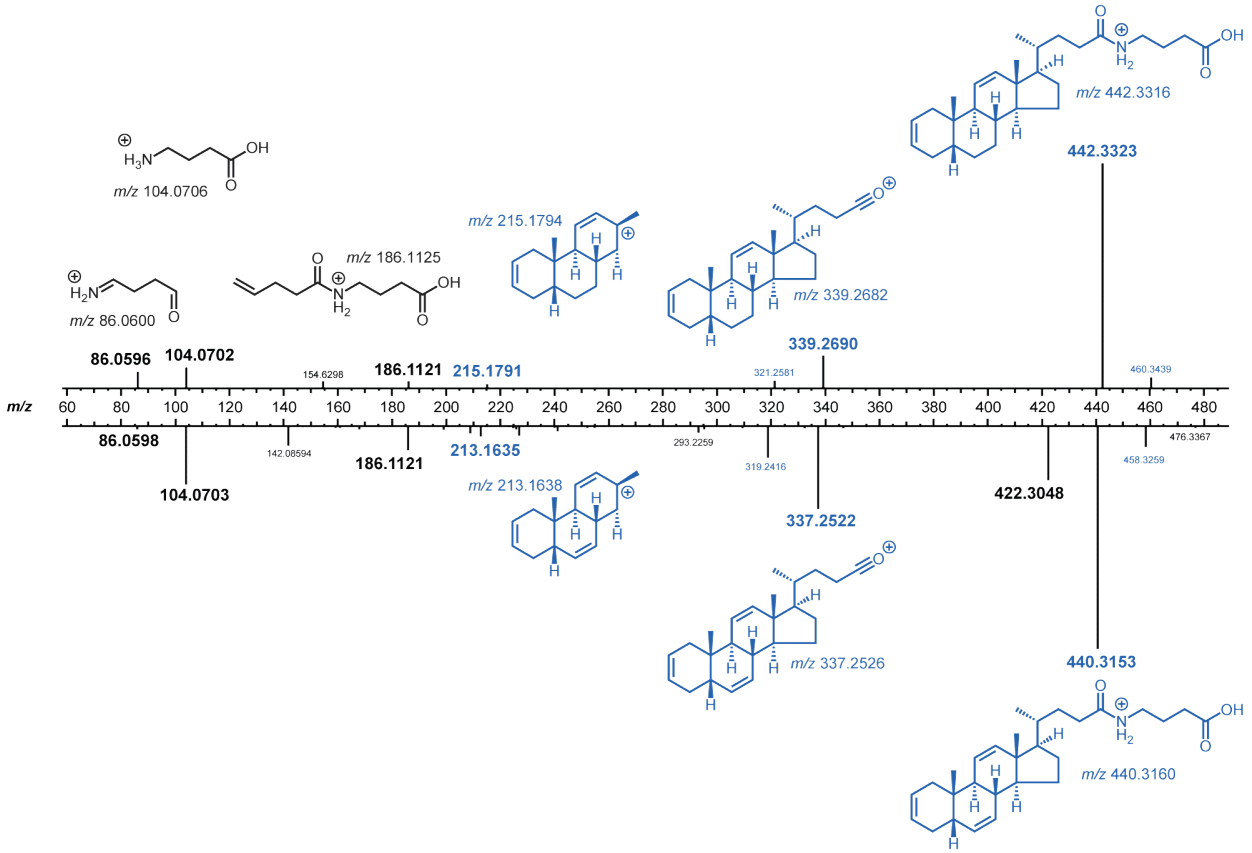

Figure S10. Mirror plot of a summed DCA-GABA (*m/z* 478.3531) MS^2 spectrum opposite a summed MS^2 spectrum representative of the three putative CA-GABA isomers (*m/z* 494.3476) observed in patient 207 feces, healthy donor feces, and healthy donor isolates *in vitro*. The 16 Dalton difference between the parent ions' *m/z* values and the -2 shifts observed in the expected MS^2 fragments between the spectra (an additional hydroxyl reduction, shown in blue) are indicative of the additional hydroxyl group that is present in the cholate steroidal core when compared to DCA. In addition, the matching MS^2 fragments at *m/z* 186.1125, *m/z* 104.0702, and *m/z* 86.0596 support assignment of this structure as a cholic acid-GABA conjugant isomer. All structural assignments for MS2 ions are putative.

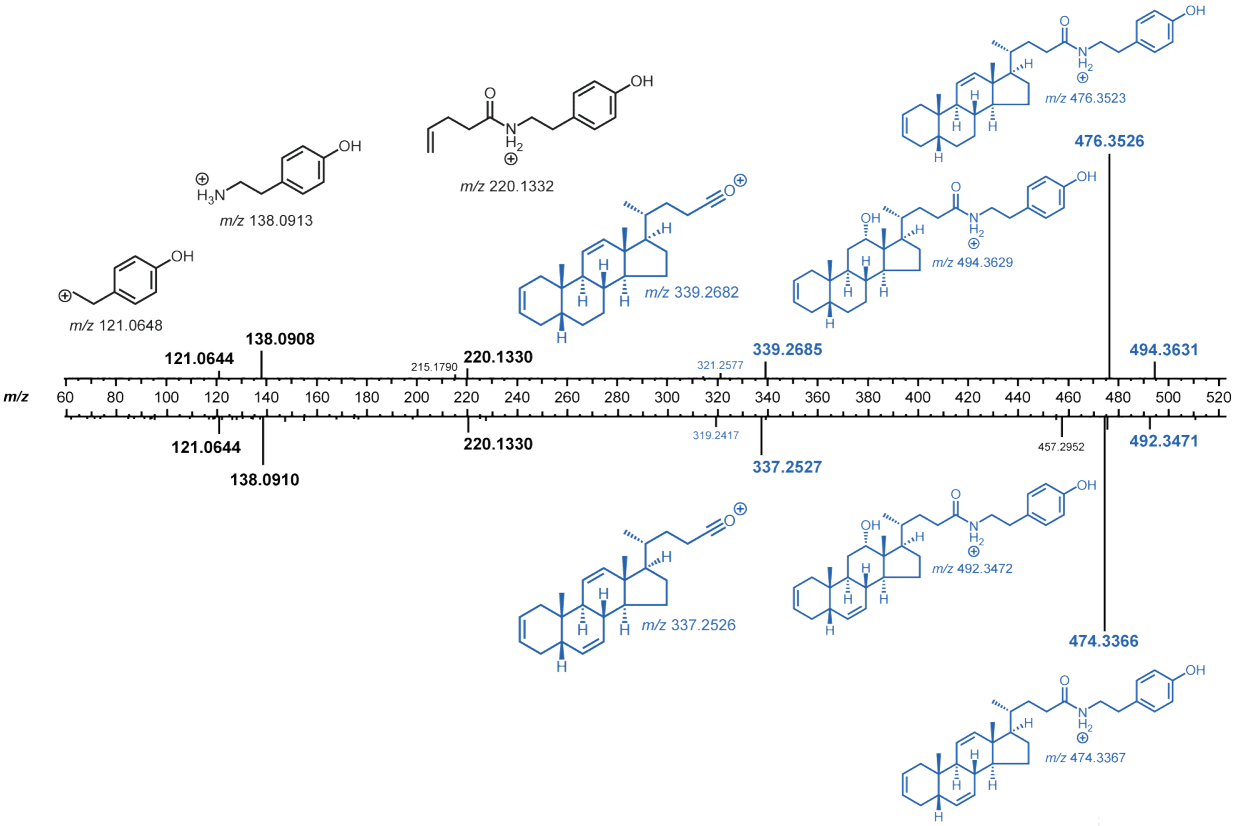

Figure S11. Mirror plot of a summed DCA-tyramine (*m/z* 512.3740) MS^2 spectrum opposite a summed MS^2 spectrum representative of the putative CA-tyramine isomer (*m/z* 528.3684) observed in healthy donor feces and healthy donor isolates *in vitro*. The 16 Dalton difference between the parent ions' *m/z* values and the -2 shifts observed in the expected MS^2 fragments between the spectra (an additional hydroxyl reduction, shown in blue) are indicative of the additional hydroxyl group that is present in the cholate steroidal core when compared to DCA. In addition, the matching MS^2 fragments at *m/z* 220.1332, *m/z* 138.0913, and *m/z* 121.0648 support assignment of this structure as a cholic acid-tyramine conjugant isomer. All structural assignments for MS2 ions are putative.

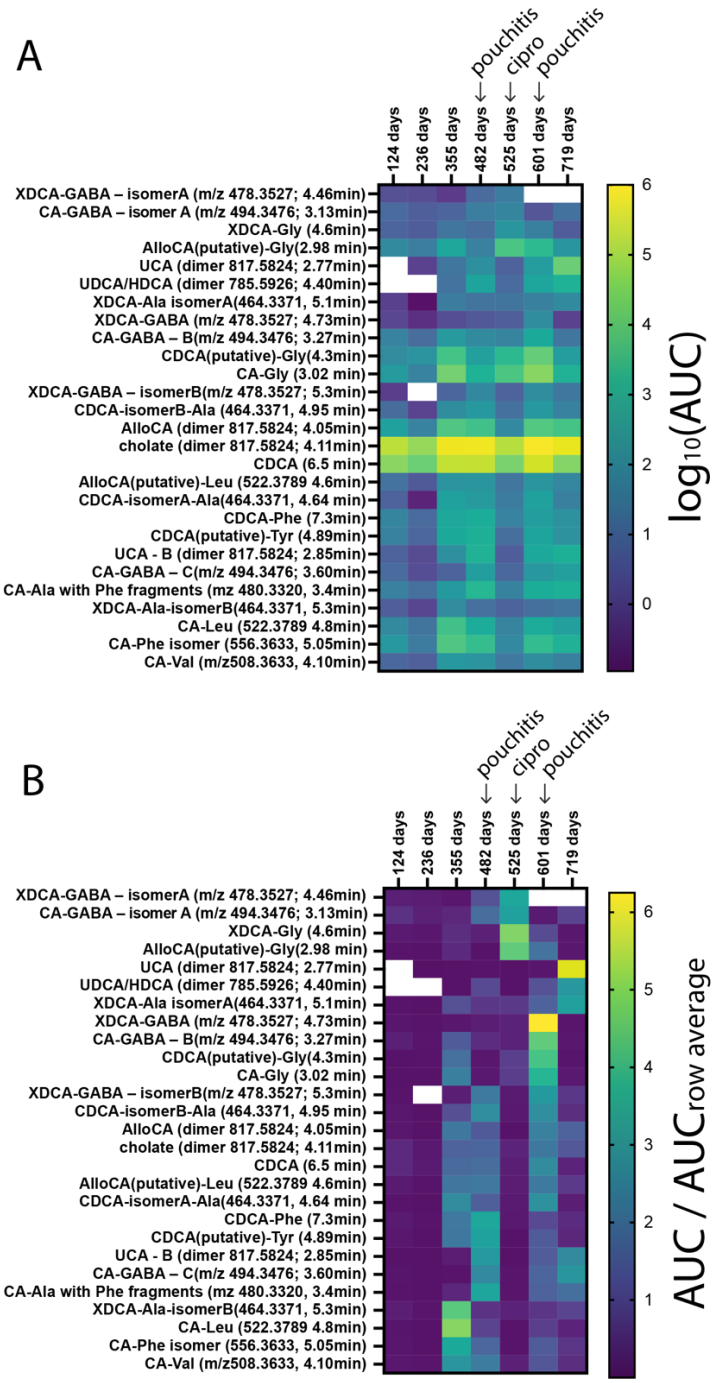

Figure S12. Heatmap illustrating the levels of unconjugated and conjugated bile acids in pouchitis patient 207 [13]. (A) Hierarchically clustered heatmap representing bile acid abundance (measured by area under the curve or AUC) from days 124 to 719 after J-pouch functionalization. The data were processed and hierarchically clustered using Cluster 3.0 [39] with an uncentered absolute correlation metric and average linkage method. (B) Hierarchically clustered heatmap of row-normalized bile acid abundance data. Here, each value is normalized to the mean AUC for its respective row, using the same clustering parameters as in (A). Timepoints where the patient was diagnosed with pouchitis or being treated with ciprofloxacin (cipro) are marked.

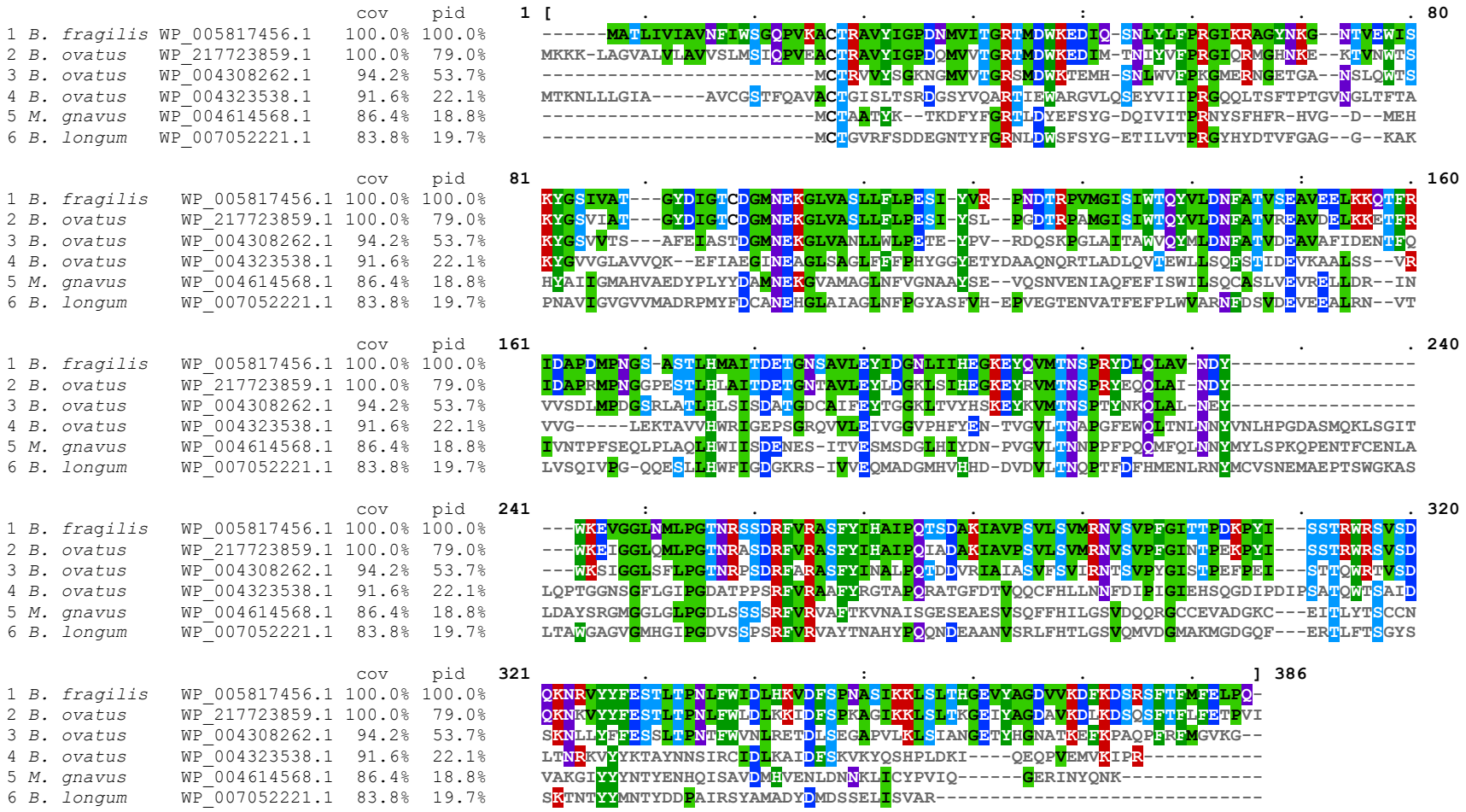

Figure S13. Multiple sequence alignment of N-terminal nucleophilic cysteine hydrolase (Ntn) enzymes (Conserved Domain Database accession cd01902) from *B. fragilis* P207 (reference sequence for this alignment; WP_005817456.1), *Mediterraneibacter gnavus* MSK15.77 (WP_004614568.1), *Bifidobacterium longum* DFI.2.45 (WP_007052221.1), and *Bacteroides ovatus* MSK22.29 (which encodes three Ntn paralogs: WP_217723859.1, WP_004308262.1, and WP_004323538.1). cov-percent coverage; pid-percent identity.

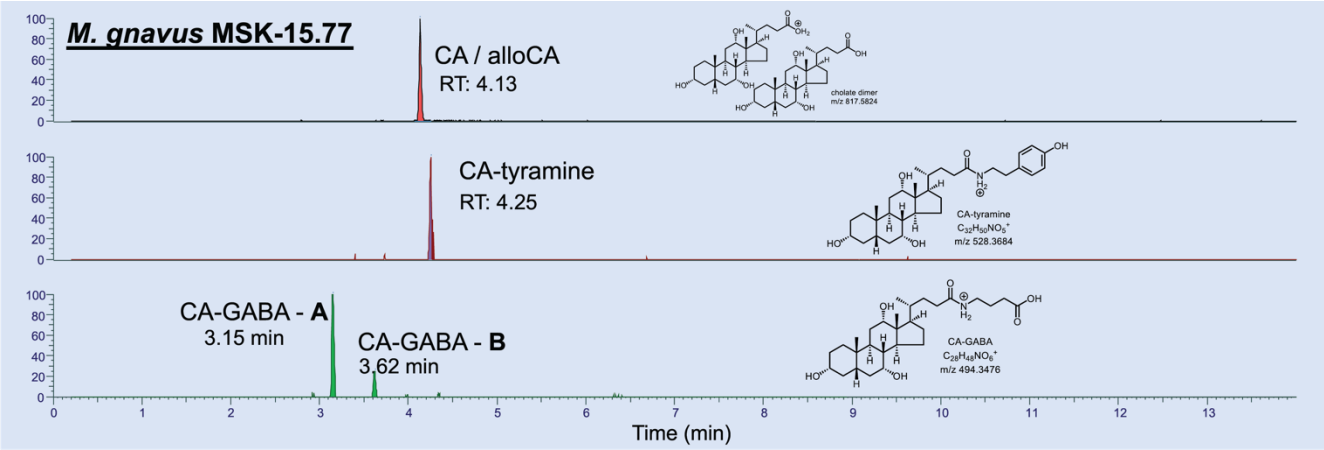

Figure S14. Incubation of *M. gnavus* strain MSK-15.77 with 0.01% (w/v) cholic acid (CA) in BHIS broth followed by separation of culture extract by liquid chromatography provides evidence for production of CA-tyramine and two species with MS/MS profiles matching CA-GABA (putative isomers).

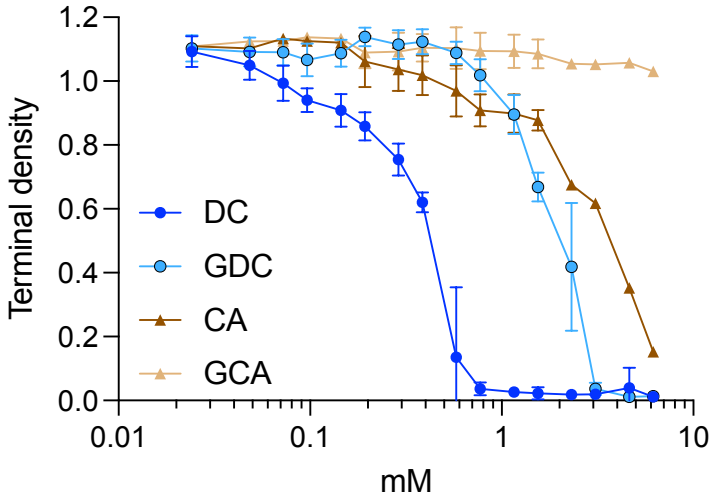

Figure S15. Glycine conjugation to DCA and CA reduces toxicity to *B. fragilis* P207 *in vitro*. Terminal density measurements (OD_{600}) of *B. fragilis* P207 (24 hours of growth) in BHIS under increasing concentrations of bile acids (DC-deoxycholic acid; GDC-glycodeoxycholic acid; CA-cholic acid; GCA-glycocholic acid). Data show five biological replicates for DC and CA, and three replicates for GDC and GCA; error bars represent standard deviation.